

NO_x versus VOC limitation of O₃ production in the Po valley: Local and integrated view based on observations

Christoph Spirig¹ and Albrecht Neftel

Swiss Federal Research Station for Agroecology and Agriculture
Zürich-Reckenholz and Liebefeld-Bern, Switzerland

Lawrence I. Kleinman

Atmospheric Sciences Division, Department of Environmental Science,
Brookhaven National Laboratory, Upton, New York

Jens Hjorth

Environment Institute, Joint Research Center of the European Commission, Ispra, Italy

Received 28 February 2001; revised 21 June 2001; accepted 26 June 2001; published 13 September 2002.

[1] We characterize the local O₃ production at an urban and a rural site in the northern part of the Po valley (Italy) during the Pianura Padana Produzione di Ozono experiment (PIPAPPO). A steady state calculation based on observations is performed to determine the local O₃ production rate, P(O₃), and its sensitivity to precursor concentrations. The urban site exhibited a strongly VOC sensitive O₃ production rate, while both VOC and NO_x sensitive conditions were observed at the rural site. In addition to the local steady state analysis, we performed one-dimensional Lagrangian model calculations that simulate conditions in the Po valley. These calculations show that the P(O₃) at the surface tends to be more VOC sensitive than the average in the mixed layer. The Lagrangian calculations are also used to determine the response of O₃ concentration to an emissions change. We compare emission control information with information on sensitivities from the local analysis. It is concluded that a local analysis of P(O₃) within the mixing layer offers useful qualitative information but tends to overestimate VOC sensitivity as judged by a comparison with an emissions-based Lagrangian model. *INDEX TERMS:* 0345 Atmospheric Composition and Structure: Pollution—urban and regional (0305); 0365 Atmospheric Composition and Structure: Troposphere—composition and chemistry; 0368 Atmospheric Composition and Structure: Troposphere—constituent transport and chemistry; *KEYWORDS:* tropospheric ozone, photooxidants, NO_x-VOC sensitivity, ozone precursors, urban pollution, photochemical modeling

Citation: Spirig, C., A. Neftel, L. I. Kleinman, and J. Hjorth, NO_x versus VOC limitation of O₃ production in the Po valley: Local and integrated view based on observations, *J. Geophys. Res.*, 107(D22), 8191, doi:10.1029/2001JD000561, 2002.

1. Introduction

[2] Tropospheric ozone concentrations are known to be highest downwind of large cities. The Po valley in northern Italy often exhibits ozone levels that are among the highest concentrations observed in Europe. The ingredients for the production of high ozone levels: nitrogen oxides (NO_x), volatile organic compounds (VOC), and solar radiation are abundant in this region. The highly industrialized and densely populated Milan metropolitan area and the extended road network around supply high emissions of VOC and NO_x [Heymann *et al.*, 1994; Klimont *et al.*, 1993]. In addition, the meteorological situation during summer months is often characterized by high-pressure conditions with high solar radiation. Wind directions are then dominated by a mesoscale breeze

induced by a heat low over the Alps, leading to a southern wind direction during daytime and a flow from north to south during the night [Lehnig *et al.*, 1996].

[3] Earlier investigations in the area observed a plume originating from Milan, in which the production of photooxidants was highly effective. Prévôt *et al.* [1997] found ozone concentrations up to 185 ppb 4–5 hours downwind of Milan. Differences in ozone concentrations between air masses within and outside the plume were as high as 100 ppb, indicating that the Milan plume can add enormously to the regional background.

[4] The PIPAPPO field experiment [Neftel *et al.*, 2002] aims to describe the spatial and temporal dynamics of the VOC versus NO_x sensitivity of the ozone production in the northern part of the Po valley. In this work we present an observation based approach to get information about the limitation of ozone formation. A steady state calculation driven by observations gives the local O₃ production rate, P(O₃) and its sensitivity to NO and VOCs, $d\ln P(O_3)/d\ln[NO]$ and $d\ln P(O_3)/d\ln[VOC]$. These quantities describe the instantaneous

¹Formerly at Atmospheric Chemistry Division, National Center for Atmospheric Research, Boulder, Colorado, USA.

chemistry at the time and place where the measurements were taken. In this case, we characterize the chemistry at two surface sites.

[5] We study how this local and instantaneous information can be related to the regional context of ozone control strategies. With a one-dimensional (1-D) Lagrangian photochemical model we simulate a situation that is representative for summer smog conditions in the Po valley. The results of these model runs are treated in the same way as the observations and used as inputs for steady state calculations. We thus get the local characteristics of the chemistry as a function of altitude. This allows us to address, if the conditions of ozone production through the depth of the boundary layer can be assessed based on surface observations.

[6] The 1-D model is also used to investigate the effects of emission changes on the ozone concentrations. This combination of local analyses and 1-D model calculations allows us to discuss the relations between local quantities that are accessible to observations and the integrated perspective, the sensitivity of O₃ concentration to its precursor emissions.

2. PIPAPO Field Experiment

2.1. Scope

[7] Earlier field experiments and model studies on the chemistry of the Milan plume indicated that the transition from VOC to NO_x sensitive regime in the plume occurs within a relatively short time [Staffelbach and Nefiel, 1997; Staffelbach et al., 1997a]. The PIPAPO experiment took place in early summer 1998 and was designed based on this experience: Major ground stations were placed along the prevailing wind direction. One was located upwind of the strongest emission sources, while the others were situated between 5 and 40 km downwind of the major emission source. According to earlier model calculations, these stations were expected to be located in different O₃ production regimes [Nefiel et al., 2002].

2.2. Measurement Sites

[8] Results from two PIPAPO measurement sites, Bresso and Verzago, will be discussed in this work. At these two sites, extensive sets of parameters were measured which allows an observation based characterization of the local ozone production.

2.2.1. Verzago

[9] Verzago is located ~35 km north of downtown Milan (Figure 1). This station has a rural character and is located slightly higher than its surroundings. The nearest major emission source is a highly congested road one kilometer northeast, connecting the cities of Como and Bergamo. There are no major emission sources nearby to the south. Therefore it is expected that the air reaching the site under prevailing southern wind directions during smog episodes is relatively undisturbed by recent emissions.

2.2.2. Bresso

[10] The second station considered is situated on a military air field in Bresso, in the northern outskirts of Milan (5 km north of downtown Milan). North of this site lies a major highway axis and just 50 m west there is another very busy street (Viale A. Grandi). For a detailed description of this site, see Aliche et al. [2002]. Bresso is expected to exhibit a strongly VOC-limited ozone production regime due to the emission sources nearby.

2.3. Measurement Methods

[11] Most of the measurements we will discuss here were performed with the same techniques at both sites and instruments are identical with those described by Staffelbach et al. [1997a]. New additions for this campaign were a modulated chemical amplifier (MCA) for peroxy radical measurements at the Verzago site and differential optical absorption spectrometers (DOAS) for measurements at the Bresso site. [Aliche et al., 2002].

[12] Table 1 summarizes the measured parameters that were used in our analyses. O₃, NO and NO₂ were measured with a commercially available system (Cranox, Ecophysics, Switzerland). O₃ was measured by UV absorption, NO by ozone chemiluminescence. NO₂ and NO_y were determined as NO by means of a photolytic and a molybdenum converter, respectively. Details about this system and calibration procedures are given by Thielmann et al. [2002].

[13] HNO₃ and HONO were collected using a parallel plate denuder (PPD) and subsequently analyzed by ion chromatography. The denuder was designed for a quantitative stripping of soluble gases [Nefiel et al., 1996; Staffelbach et al., 1997a].

[14] Peroxyacetyl nitrate (PAN) was measured with a commercial system (LPA-4 PAN analyzer, Scintrex Unisearch, Canada), a gas chromatograph combined with a Luminol chemiluminescence detector, measuring thermally decomposed PAN as NO₂.

[15] H₂O₂ was collected with a Nafion denuder and measured with fluorescence detection. The system has a built-in gas phase calibration source and is described in detail by Sigg et al. [1992].

[16] At the Verzago site, HCHO was collected in a Nafion membrane diffusion scrubber and analyzed with fluorescence detection. At the Bresso site, HCHO was measured by DOAS [Aliche et al., 2002].

[17] Acetone and acetaldehyde were sampled on cartridges containing 2,4-dinitrophenylhydrazine (DNPH) coated silica and analyzed a few days after collection by the Norwegian Institute for Air Research (NILU), Kjeller, Norway, by reversed phase HPLC using UV detection.

[18] Hydrocarbons (C₄-C₁₁) were measured with a commercial gas chromatograph (airmVOC 1010, Airmotec, Switzerland). The instrument was run in a quasi-continuous mode. Hydrocarbons (HC) were first preconcentrated on Carbosieve/Carbotrap cartridges at ambient temperature, then thermally desorbed, cryofocused on a short column containing Carbopack B at temperatures below 0°C and finally injected onto a BGB 2.5 capillary column. Details about the hydrocarbon measurements at both sites are given by Gruebler [1999].

[19] HONO was measured with a DOAS system at the Bresso site. The instrument and the significance of HONO at this site are discussed in detail by Aliche et al. [2002] and Stutz et al. [2002].

[20] Peroxy radicals were measured with a modulated chemical amplifier (MCA) instrument that has been described in detail elsewhere [Cantrell et al., 1984; Hastie et al., 1991]. The method is based on a chain reaction producing NO₂, initiated by the reaction of HO₂ radicals with NO in a CO/NO/air system; NO₂ is then measured as a proxy of the HO₂ radicals. Since most organic peroxyradicals produce HO₂ by their reaction with NO and O₂, the instrument will also respond to these radicals. The MCA used in this study was built at the Institute

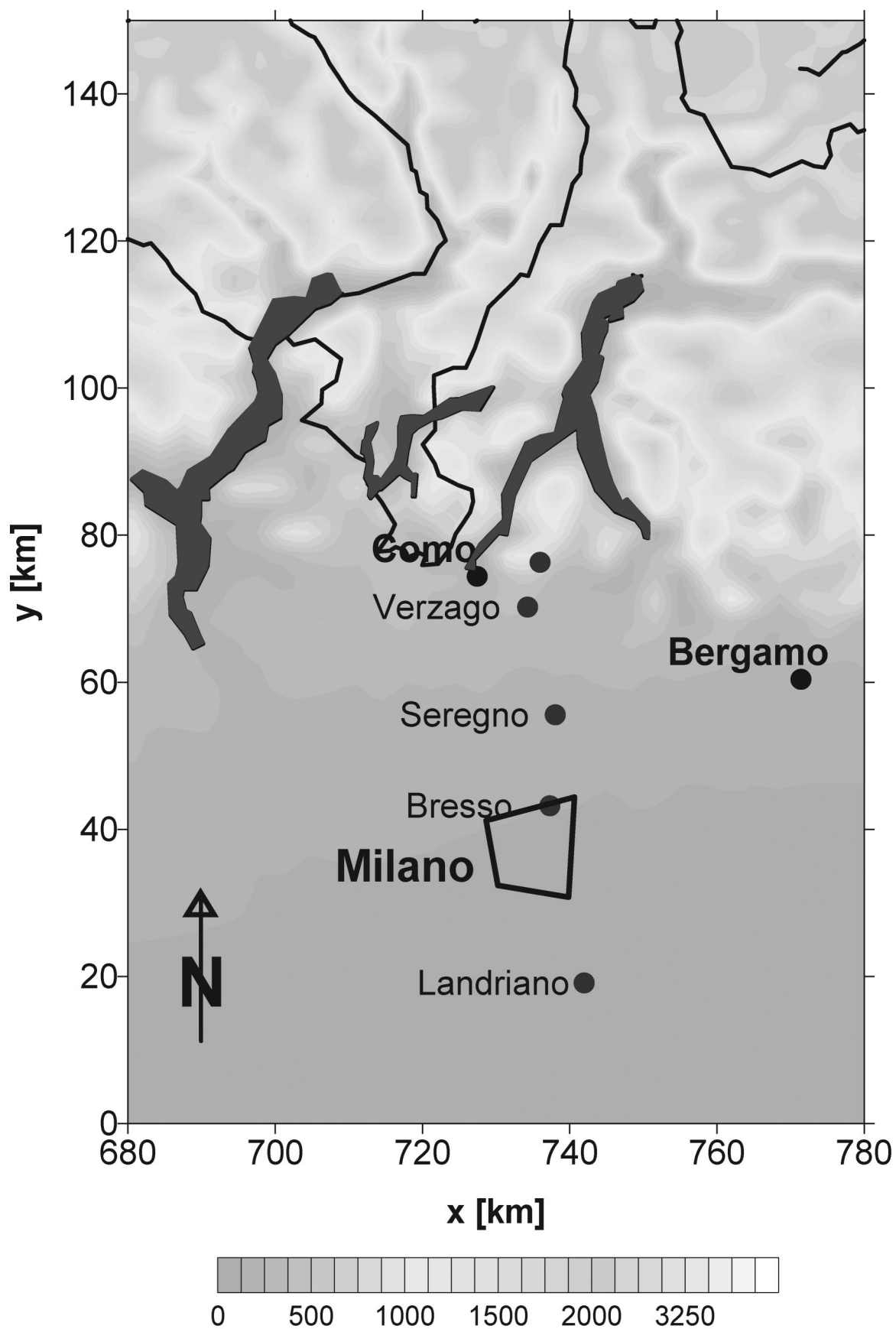


Figure 1. PIPAPO ground stations. Color scale indicates altitude above sea level (m). See color version of this figure at back of this issue.

Table 1. Instrumentation at the Verzago and Bresso Sites^a

Species	Analytical Method	Detection Limit	Time Resolution
<i>Verzago</i>			
O ₃	UV absorption	3 ppb	20 s
NO	chemiluminescence	23 ppt	20 s
NO ₂	chemiluminescence with photolytical converter	23 ppt	20 s
NO _x	chemiluminescence with molybdenum converter	23 ppt	20 s
Hydrocarbons (C ₄ -C ₁₁)	gas chromatograph with FID	20 ppt (C ₄)	30 min
H ₂ O ₂	monitor based on gas injection	100 ppt	2 min
HNO ₃	parallel plate denuder with IC	10 ppt	60 min
HONO	parallel plate denuder with IC	5 ppt	60 min
PAN	GC combined with Luminol detection	100 ppt	30 min
HCHO	Coil collection with fluorescence	0.5 ppb	60 min
CH ₃ CHO	DNPH cartridges and HPLC	0.5 ppb	200 min
Acetone	DNPH cartridges and HPLC	0.5 ppb	200 min
CO	nondispersive IR absorption	50 ppb	1 min
Peroxy radicals	(see text, section 2.3)		
<i>Bresso</i>			
O ₃	UV absorption	2 ppbv	20 s
NO	chemiluminescence	50 ppt	20 s
NO ₂	chemiluminescence with photolytical converter	50 ppt	20 s
NO _x	chemiluminescence with molybdenum converter	50 ppt	20 s
Hydrocarbons (C ₄ -C ₁₁)	gas chromatograph with FID	20 ppt (C ₄)	30 min
HCHO	DOAS	1.6 ppb	5 min
HONO	DOAS	0.2 ppb	5 min
CO	nondispersive IR absorption	50 ppb	1 min

^aHourly means were used as inputs for steady state calculations.

of Environmental Physics at the University of Bremen, Germany, and uses detection of NO₂ by measurement of the chemiluminescence of its reaction with a luminol solution. The concentrations of NO and CO applied in this system were 4 ppmV and 9%, respectively.

[21] The sensitivity of the chemical amplifier depends on the reaction chain length, which was determined using a known radical concentration generated by the photolysis of water in air to form HO and HO₂ radical as described by *Schultz et al.* [1995]. The average measured chain length during the campaign was 182 with a standard deviation of 26. Chain length and NO₂ calibrations were performed daily, apart from 5 June, where the data of the subsequent calibration were used.

[22] It has recently been shown that the response of the MCA to HO₂ as well as to organic peroxy radicals decreases significantly with increasing humidity of the air that is sampled, apparently due to a combination of increased wall losses and a water dependence of the gas phase chemistry [*Mihele and Hastie*, 1998]. The relationship between chain length and relative humidity is temperature dependent. In order to allow a correction of measured data for this humidity effect, the chain length calibration of the MCA was performed at different temperatures and relative humidity levels. For typical daytime relative humidity and temperature at Verzago during the measurement period (40–60% RH, 26°C), this correction is in the range between a factor of 2 and 2.5.

[23] The random error on the RO₂ measurements is mainly due to fluctuations in the detected NO₂ signal (most of the NO₂ arriving at the detector comes from the titration of ozone by NO in the instrument). For the measurements reported here this random “noise” level corresponds typically to approximately 10 pptV [RO₂] (data are averaged over 10 minutes). The size of other, potential sources of measurement errors can only be tentatively estimated. On the basis of the observed variations we estimate that changes in chain length during a day and uncertainties on the chain length calibration will cause

a 20% uncertainty on the measurements, and that the uncertainty on the correction for the effects of humidity will be approximately 30%. It must also be taken into account that the response of the MCA to organic peroxy radicals is not exactly the same as the response to HO₂ radicals. A recent study [*Ashbourn et al.*, 1998] has shown that the response of an MCA instrument to a series of organic peroxy radicals was between 6 and 38% higher than the response to HO₂. This difference in sensitivities may add another 15% uncertainty. Thus the overall measurement uncertainty is estimated to be a 10 pptv baseline noise combined with an uncertainty, proportional to the measured concentrations, of ~39% (calculated as the geometric mean of the three contributions).

2.4. Intensive Observation Periods

[24] Two intensive observation periods (IOP) took place. They were chosen to cover high ozone episodes, i.e., days with high solar radiation and low wind speeds. For details about the weather conditions, see *Nefel et al.* [2002]. The last days of a longer period with warm and sunny weather were 12 and 13 May. Wind directions on these days corresponded almost ideally to the situation desired for the PIPAPO experiment. Especially on 13 May, winds blew directly from the south, and the measurement sites were in a line downwind of the strongest emission sources. Clear sky and high temperatures led to an effective photochemistry in the boundary layer and a maximum ozone concentration of 195 ppb (half hour mean) was reached at Verzago.

[25] The second IOP from 1 to 10 June showed a somewhat unsteady situation with wind directions that often differed from the desired flow from south to north. The days were warm, but not always cloudless. Nevertheless, ozone production in the Po valley was still considerable from 2 till 4 June, when ozone maximums up to 150 ppb were measured in the foothills of the Alps, 40 km north of Milan. The second IOP was not a continuous high ozone episode. Showers occurred in the morning on 5 June north of Milan and an almost contin-

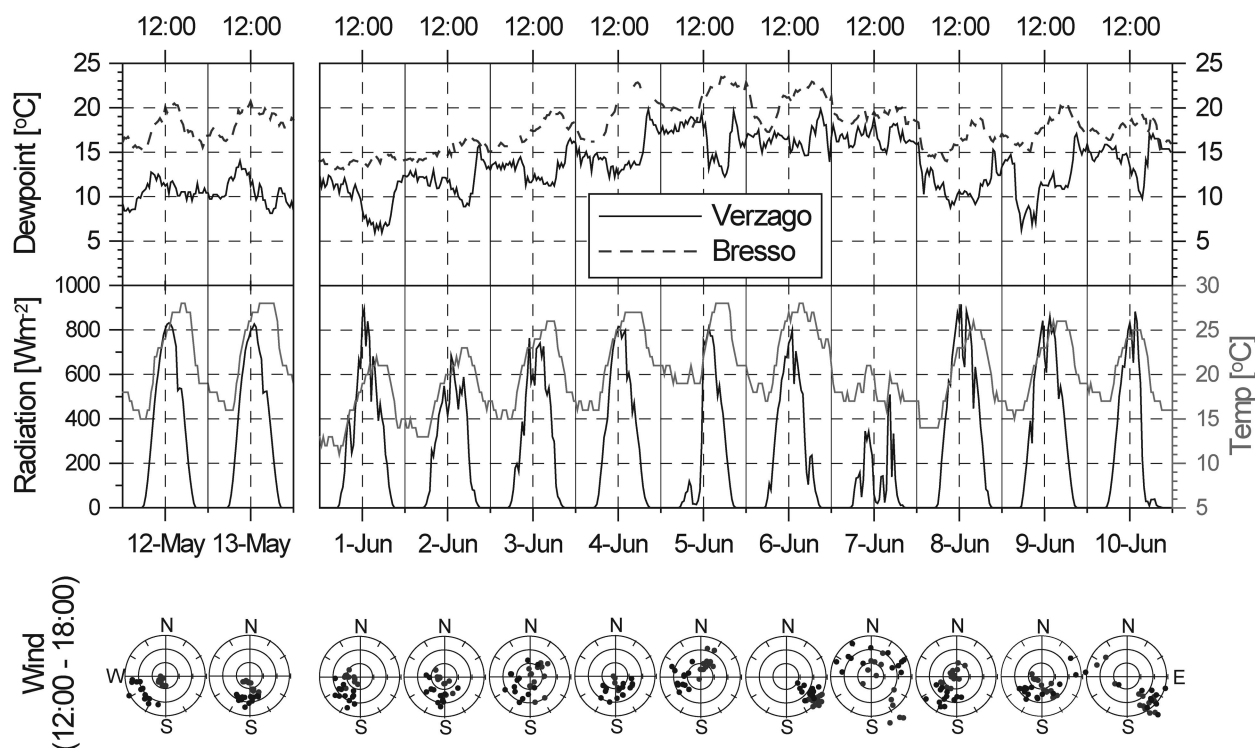


Figure 2. Humidity, temperature (red), incoming radiation, and afternoon winds during the IOPs. Temperature and radiation are shown for Verzago only. See color version of this figure at back of this issue.

uous rainfall on 7 June terminated the first half of this IOP. From 8 through 10 June, weather conditions were again favorable for high ozone production, although somewhat limited by clouds. Figure 2 gives an overview on the meteorological situation during the two IOPs.

[26] As can be seen in Figure 3, the different character of the two sites in terms of pollution is evident; the urban site Bresso with strong variations in concentrations of primary emissions and the rural station of Verzago with generally lower concentrations in VOC, NO_x, and CO, but higher levels of ozone.

[27] In the afternoon on 13 May, 4 June, and 9 June the rural site at Verzago exhibited slightly higher concentrations of VOC and NO_y for a short time period. Since the NO_x concentrations at Verzago do not show this behavior, it is an indication that a heavily polluted and photochemically aged air mass arrived at Verzago at those periods. This observation was particularly pronounced in the afternoon of 13 May, the day with the highest ozone concentration at Verzago during the whole measurement campaign. Note that there are a few occasions (mainly during the night or in the early morning) at Bresso where NO_x measurements exceed the values of NO_y. The reason is probably an incomplete conversion in the molybdenum converter (A. Thielmann, personal communication, 2001) at very high NO_x concentrations. The data of interest for this study, i.e., daytime concentrations, are free of such artifacts [Thielmann *et al.*, 2002].

3. Models

[28] We use two model tools for our analyses about the limitation of ozone production: Steady state calculations for the characterization of local and instantaneous quantities and

a 1-D photochemical model for studying the relation between emission changes and regional ozone concentration.

3.1. Steady State Approximation (SSA)

[29] Concentrations of odd-H radicals (odd hydrogen = OH + HO₂ + RO₂, whereas RO₂ stands for any organic peroxy radicals) were estimated with a radical steady state approximation (SSA) [Staffelbach *et al.*, 1997a]. Owing to their short lifetimes, the radical species OH, HO₂, and RO₂ are assumed to be in a steady state, and their concentrations can be determined using a system of equations:

$$\frac{d[\text{OH}]}{dt} = P_{\text{OH}} - [\text{OH}] \sum_i k_i [S_i] = 0 \quad (1)$$

$$\frac{d[\text{HO}_2]}{dt} = P_{\text{HO}_2} - [\text{HO}_2] \sum_j k_j [S_j] - 2k_{\text{peroxid}} [\text{HO}_2]^2 = 0 \quad (2)$$

$$\frac{d[\text{RO}_2]}{dt} = P_{\text{RO}_2} - [\text{RO}_2] \sum_j k_j [S_j] - 2k_{\text{o-peroxid}} [\text{RO}_2]^2 = 0, \quad (3)$$

where P_{OH} , P_{HO_2} , and P_{RO_2} are the production rates of OH, HO₂, and RO₂, respectively. S_i , S_j , and S_j denote (radical or nonradical) species that act as reaction partners in sink reactions of OH, HO₂, and RO₂, respectively. The concentrations of the non-radical reaction partners were constrained to measured concentrations. The Steady state equations (1–3) were solved by iteration for OH, HO₂, and RO₂. Table 2 shows all radical reactions that were considered in this SSA. Details

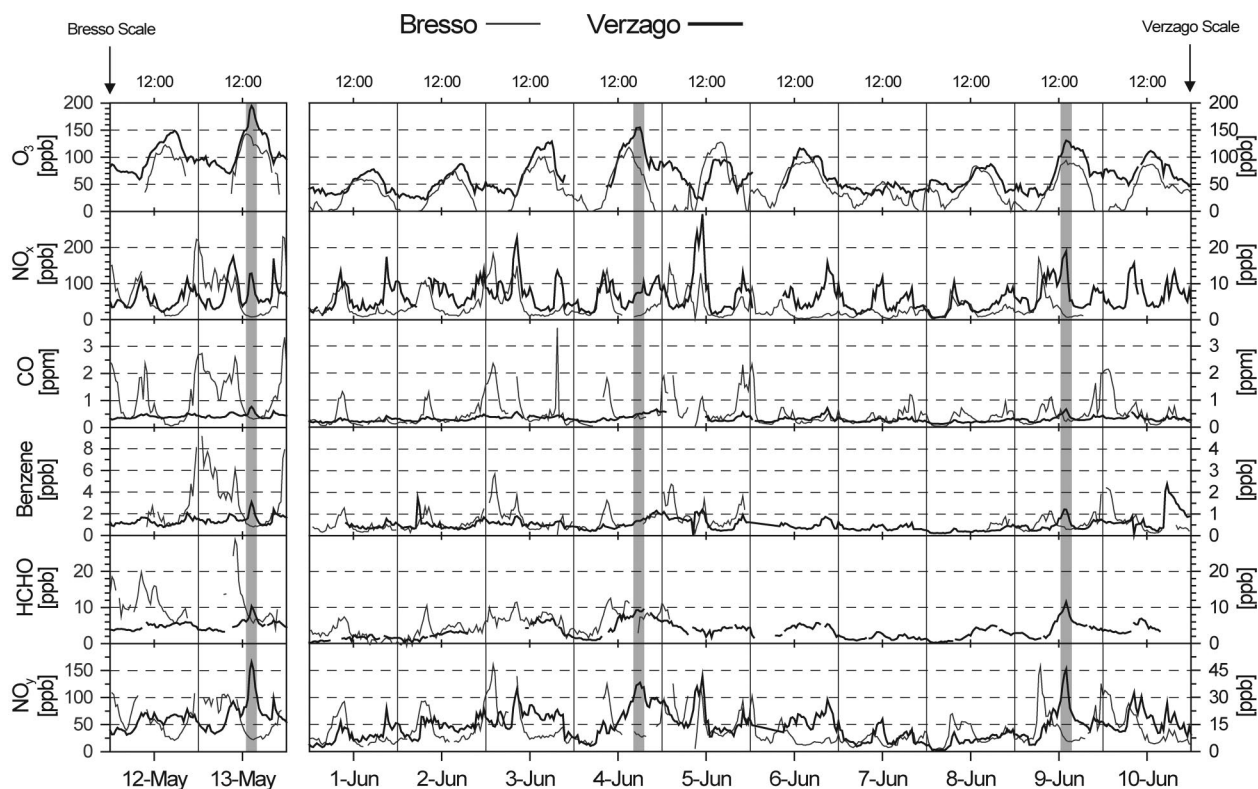


Figure 3. Selected measurements at Bresso and Verzago during both IOPs. Note the different scales at the two sites for NO_x, NO_y, and benzene. NO_x concentrations at Bresso during the afternoons of May 13, June 4, and June 9 are 35 to 40% of NO_y, whereas at Verzago the NO_x to NO_y ratio is 20 to 25%. See color version of this figure at back of this issue.

about the choice of reaction rates are given by *Staffelbach et al.* [1997a]. Some minor modifications were made for this work and are briefly described here.

[30] The SSA was performed in two variations; with NO and NO₂ input concentrations fixed to the measured values, and with only NO taken from measurements. In the later case, NO₂ was determined by including it in the iteration, where it was calculated as

$$[\text{NO}_2] = [\text{NO}]([\text{O}_3]k_{\text{O}_3} + [\text{HO}_2]k_{\text{HO}_2} + [\text{RO}_2]k_{\text{RO}_2})/j_{\text{NO}_2}, \quad (4)$$

with $k_{\text{O}_3} = 1.8\text{E} - 12 \times \exp(-1370/T) \text{ cm}^3 \text{ molecules}^{-1} \text{ s}^{-1}$, and other rate constants according to Table 2.

[31] Photolysis rates were calculated with the Tropospheric Ultraviolet and Visible Radiation model (TUV, V4.1a) [*Madronech and Flocke, 1999*]. We calculated clear-sky photolysis rates for the Po valley with consideration of total ozone concentrations as obtained from measurements of Earth Probe TOMS (NASA). At Verzago, J_{NO_2} measurements were available for the first IOP [*Thielmann et al., 2002*]. These observed values were used to calculate j values for other photolysis reactions (j_x) by scaling the clear-sky TUV model predictions ($j_x(\text{TUV})$); i.e.,

$$j_x = j_x(\text{TUV}) \frac{j_{\text{NO}_2}(\text{obs.})}{j_{\text{NO}_2}(\text{TUV})} \quad (5)$$

When j_{NO_2} observations were not available, TUV photolysis rates were scaled by the ratio of measured to theoretical total solar irradiance as derived from zenith angles.

[32] For the rate of the reaction $\text{VOC} + \text{OH}$ a mean of $1.2 \times 10^{-12} \text{ mol cm}^{-3} \text{ s}^{-1}$ (Verzago) and $1.5 \times 10^{-12} \text{ mol cm}^{-3} \text{ s}^{-1}$ (Bresso) was chosen. These values correspond to the averaged reactivities of the VOC mix (with VOC expressed in units of carbon concentration) as estimated from the HC measurements at Verzago and Bresso. Reaction rate constants of individual HCs were taken from *Atkinson et al.* [1992]. Since the HC measurements at these sites included only C₄-C₁₁, an approximation was made for the contribution of C₂ and C₃ hydrocarbons. Based on measurements of these compounds at the nearby site of Colma del Piano, we estimated an addition of 20% to the total OH reactivity from this group. Because of its high reactivity and unique emission source, isoprene is included explicitly in our SSA and not as part of the VOC group. Among the oxygenated VOCs, formaldehyde, acetaldehyde, and acetone were treated explicitly in our SSA. Since the VOC group does not include the contribution of other oxygenated VOC, our reaction rate for this lumped group certainly reflects a lower limit estimate.

[33] Of the peroxides included in the SSA, (H₂O₂ and CH₃OOH), only H₂O₂ was continuously measured in this campaign. Considering the small influence of CH₃OOH on the results of the SSA, we used a constant concentration of 330 ppt, a value based on the experience of detailed peroxide measurements in an earlier experiment in the area. [*Staffelbach et al., 1997a*].

[34] The radical concentrations estimated by SSA were used to calculate instantaneous ozone production rates at both measurement sites. Ozone production, $P(\text{O}_3)$, is assumed to be determined by the reactions,

Table 2. List of Reactions Considered in the Steady State Approximation (SSA)

Reaction						Reaction Rate Constant ^a	
OH sources							
HO ₂	+	NO	→	OH	+	NO ₂	8.5E-12
O ₃	+	HO ₂	→	OH	+	2O ₂	2.1E-5
O ₃	+	<i>hν</i>	→	2 OH	+	O ₂	2.31E-5
HONO	+	<i>hν</i>	→	OH	+	NO	1.77E-3
H ₂ O ₂	+	<i>hν</i>	→	2 OH			5.71E-6
CH ₃ OOH	+	<i>hν</i>	→	HCHO	+	HO ₂	4.41E-6
CH ₃ OOH	+	OH	→	HCHO	+	H ₂ O	2.2E-12
OH sinks							
Isoprene	+	OH	→	RO ₂	+	products	1.0E-10
VOC	+	OH	→	RO ₂	+	products	1.5E-12
HCHO	+	OH	→	CO	+	HO ₂	1.0E-11
CO	+	OH	→	CO ₂	+	HO ₂	2.4E-13
NO ₂	+	OH	→	HNO ₃	+	M	1.1E-11
HO ₂	+	OH	→	O ₂	+	H ₂ O	1.1E-10
CH ₄	+	OH	→	RO ₂	+	H ₂ O	6.7E-15
O ₃	+	OH	→	O ₂	+	HO ₂	7.0E-14
OH	+	NO	→	HONO	+	M	4.8E-12
OH	+	H ₂	→	HO ₂	+	H ₂ O	7.2E-15
H ₂ O ₂	+	OH	→	H ₂ O	+	HO ₂	1.7E-12
CH ₃ OOH	+	OH	→	RO ₂	+	H ₂ O	5.2E-12
CH ₃ OOH	+	OH	→	HCHO	+	H ₂ O	2.2E-12
CH ₃ COCH ₃	+	OH	→	RO ₂	+	H ₂ O	2.1E-13
HONO	+	OH	→	NO ₂	+	H ₂ O	4.9E-12
CH ₃ CHO	+	OH	→	RO ₂	+	H ₂ O	1.6E-11
HNO ₃	+	OH	→	NO ₃	+	H ₂ O	1.4E-13
HO ₂ sources							
CO	+	OH	→	CO ₂	+	HO ₂	2.4E-13
RO ₂	+	NO	→	NO ₂	+	HO ₂	7.7E-12
HCHO	+	<i>hν</i>	→	2 HO ₂	+	CO	2.37E-5
OH	+	H ₂	→	HO ₂	+	H ₂ O	7.2E-15
HCHO	+	OH	→	CO	+	HO ₂	1.0E-11
CH ₃ OOH	+	<i>hν</i>	→	HCHO	+	HO ₂	6.71E-7
CH ₃ CHO	+	<i>hν</i>	→	RO ₂	+	HO ₂	4.19E-6
RO ₂	+	RO ₂	→	2 HO ₂	+	products	3.5E-13 × 0.5
O ₃	+	OH	→	O ₂	+	HO ₂	7.0E-13
H ₂ O ₂	+	OH	→	H ₂ O	+	HO ₂	1.7E-12
HO ₂ sinks							
O ₃	+	HO ₂	→	OH	+	2 O ₂	2.1E-15
NO	+	HO ₂	→	OH	+	NO ₂	8.5E-12
RO ₂	+	HO ₂	→	products			6.0E-12
OH	+	HO ₂	→	O ₂	+	H ₂ O	1.1E-10
HO ₂	+	HO ₂	→	H ₂ O ₂			5.0E-12
RO ₂ sources							
Isoprene	+	OH	→	RO ₂	+	products	1.0E-10
VOC	+	OH	→	RO ₂	+	products	1.5E-12
CH ₄	+	OH	→	RO ₂	+	H ₂ O	6.7E-15
CH ₃ COCH ₃	+	OH	→	RO ₂	+	H ₂ O	2.1E-13
CH ₃ OOH	+	OH	→	RO ₂	+	H ₂ O	5.2E-12
CH ₃ CHO	+	OH	→	RO ₂	+	H ₂ O	1.6E-11
PAN	→		→	RO ₂	+	NO ₂	5.9E-04
CH ₃ CHO	+	<i>hν</i>	→	RO ₂	+	HO ₂	4.19E-6
RO ₂ sinks							
RO ₂	+	NO	→	NO ₂	+	HO ₂	7.6E-12
RO ₂	+	RO ₂	→	2 HO ₂	+	products	3.5E-13
			→	products			3.5E-13
RO ₂	+	HO ₂	→	products			6.0E-12
RO ₂	+	NO ₂	→	products			1.1E-11 ^b

^aRead 8.5E-12 as 8.5×10^{-12} . Rate constants at 298 K in cm³ molecule⁻¹ s⁻¹ for bimolecular reactions and in s⁻¹ for photolysis reactions. Photolysis rates are given for 12 May 1200 UTC, clear-sky conditions.

^bActual rate was fixed to the thermal decomposition rate of PAN.



since subsequent NO₂ photolysis and the reaction of O(³P) atoms with oxygen are reasonably fast. With the peroxy radical concentrations obtained from the SSA, P(O₃) is thus calculated as

$$P(\text{O}_3) = [\text{NO}](k_1[\text{HO}_2] + k_2[\text{RO}_2]). \quad (6)$$

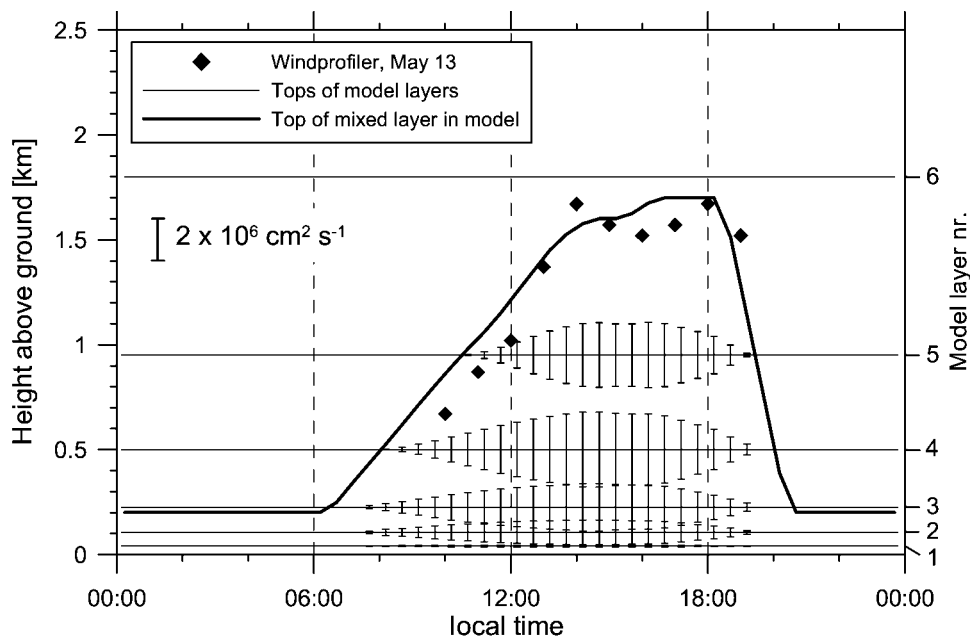


Figure 4. Mixing layer height and eddy coefficients (vertical bars) as applied in 1-D model runs. Diamonds are mixing layer heights as derived from wind profiler measurements at Seregno on May 13.

[35] The sensitivity of the instantaneous O₃ production on NO_x and VOC concentrations can be described by comparing radical sinks and sources. Kleinman *et al.* [1997] showed that the sensitivity can be derived from a single parameters L_N/Q , where Q denotes the odd-H production and L_N is the loss rate of free radicals caused by reactions with NO_x.

[36] In our calculations, Q consists of the photolysis reactions of O₃, HCHO, H₂O₂, HONO, and CH₃CHO (acetaldehyde). L_N is approximated by the reaction OH + NO₂ → HNO₃. Formation of organic nitrates from reaction of RO₂ radicals with NO is a minor channel averaged over the observed mixture of VOCs and is ignored. PAN is assumed to be in steady state so that it is neither a source or sink of radicals. The effects of this approximation are discussed in section 5. Relative sensitivities of the ozone production ($d\ln P_{O_3}/d\ln[NO_x]$) and $d\ln P_{O_3}/d\ln[HC]$ can then be expressed as simple functions of L_N/Q [Kleinman *et al.*, 1997]:

$$\frac{d\ln P(O_3)}{d\ln[NO_x]} = \frac{1 - \frac{3}{2} \frac{L_N}{Q}}{1 - \frac{1}{2} \frac{L_N}{Q}} \quad (7)$$

$$\frac{d\ln P(O_3)}{d\ln[HC]} = \frac{\frac{1}{2} \frac{L_N}{Q}}{1 - \frac{1}{2} \frac{L_N}{Q}} \quad (8)$$

VOC-sensitive conditions are characterized by a value of L_N/Q greater than 0.5, whereas a NO_x-sensitive ozone production exhibits a ratio smaller than 0.5. Relative sensitivities have a value of 1 if an $n\%$ change in [NO_x] or [VOC] results in an $n\%$ change in the ozone production [Kleinman, 2000].

3.2. One-Dimensional Lagrangian Model

3.2.1. Model Description

[37] We conducted our calculations with the Harvard photochemical trajectory model. This model has been applied be-

fore to various tropospheric chemistry situations [Fan *et al.*, 1994; Jacob *et al.*, 1995; Staffelbach *et al.*, 1997b]. The chemical mechanism is identical with the one used by Staffelbach *et al.* [1997b] and is based on the compilation of kinetic and photochemical data by Atkinson *et al.* [1992] and Moore *et al.* [1992]. It includes more than 200 species and 600 reactions. Dry deposition of O₃, NO_y species, peroxides, carbonyls, and SO₂ were parameterized by specifying deposition velocities [Staffelbach *et al.*, 1997b]. Radiation is calculated with a six-stream code for the Rayleigh scattering atmosphere at 45.7°N (latitude of Verzago equal to 45.77°N). The solar declination was set to 18.2° corresponding to 13 May. The model simulates the atmospheric boundary layer with six layers, which have increasing dimensions with altitude. The tops of the six layers are at 40, 105, 225, 500, 950, and 1800 m above ground. Movement of an air mass is simulated by varying emissions and vertical mixing. Mixing layer depth was set to 200 m at nighttime and increases during the day to 1700 m as shown in Figure 4. The estimates of the mixing layer heights from 0800 to 1800 hours compare reasonably well with the heights determined from measurements with a windprofiler, which was operated at Seregno (by the Swiss Meteorological Institute, SMI). Vertical exchange between the layers is simulated with eddy diffusion coefficients, also shown in Figure 4.

3.2.2. Emission Data

[38] Regione Lombardia Network prepared an hourly resolved emission inventory for the Milan area with a grid size of 3 by 3 km [Martilli *et al.*, 2002]. The inventory contains emissions of NO_x, CO, SO₂, and 32 classes of VOC. From this database we calculated the emissions along pathways of air masses reaching the site of Verzago on 13 May. A total of seven model runs were made simulating air masses arriving at Verzago between 1030 and 1830 (local time). The routes of the air masses were approximated by a backwards integration of hourly wind measurements. Two representative surface observations were used for this purpose, data from Verzago and the Brera tower in downtown Milan. Since these surface measure-

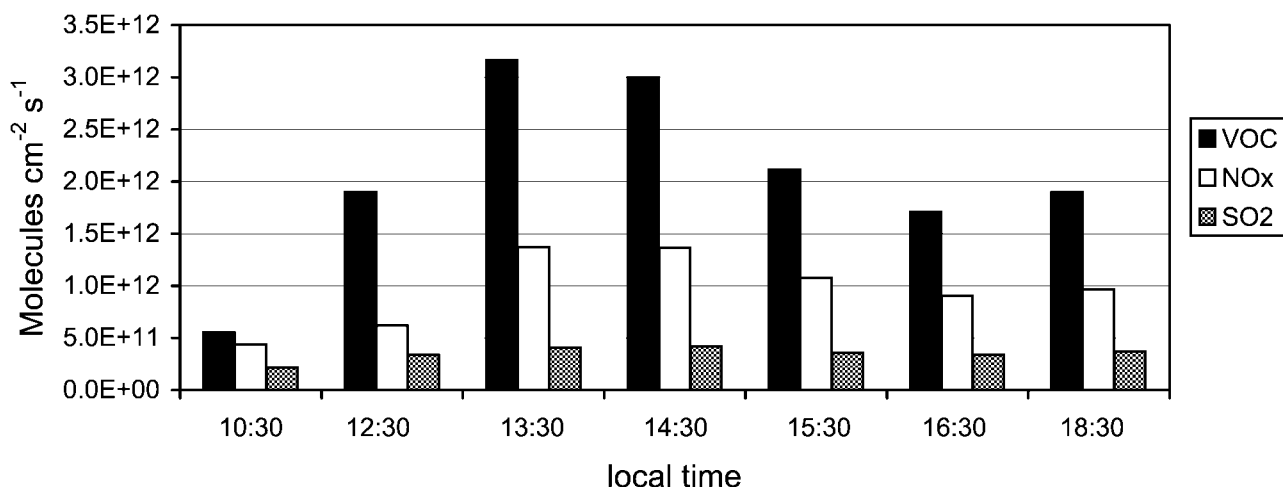


Figure 5. Mean emission strengths used in model trajectories. The trajectories are denoted by the arrival times at the Verzago site.

ments would represent too low velocities for the boundary layer, measurements at 400 m above ground from the wind profiler in Seregno were included as a third wind data set. The horizontal speed of the air parcel at time t was calculated as the weighted mean of the three measured wind vectors. The weighting of each measurement was taken inversely proportional to the distance between air parcel and measurement station; i.e.,

$$V_{\text{emp}}(t) = \sum_{i=1}^3 f_i \begin{pmatrix} u_i(t) \\ v_i(t) \end{pmatrix},$$

with V_{emp} being the empirical speed of air parcel at time t , f_i being the weighting factor for wind measurement at site i , $\sum f_i = 1$, and u_i , v_i being the horizontal wind components from measurements.

[39] We averaged the emissions over 3×3 grid cells, leading to an effective emission resolution of 9×9 km to take into account horizontal diffusion. An overview on the emission strengths of the trajectories is shown in Figure 5.

[40] Model runs lasted 48 hours and were started at midnight. Initial concentrations were taken in accordance to earlier model studies in this area [Staffelbach *et al.*, 1997b]. The simulation of the first day was not used for interpretation, but served as a prerun in order to get a consistent field of initial concentrations for the second day.

4. Model Predictions for Verzago and Bresso

[41] We start with the description of the local ozone production rate at both ground stations. These are results of calculations with the SSA. The 1-D photochemical model is afterwards used to study the relation between these local quantities and the regional and integrated perspective of ozone concentration sensitivities.

4.1. Local Analysis

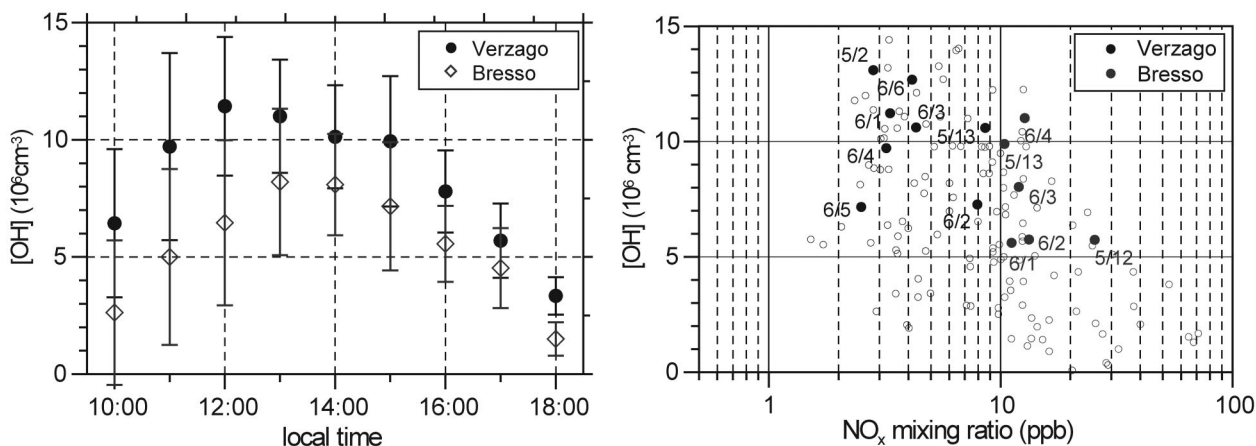
4.1.1. Radical Concentrations

[42] Figure 6 shows the calculated OH-radical concentrations of Verzago and Bresso. Mean noon OH concentrations are 1.2×10^7 molecules cm^{-3} at Verzago and 9×10^6 molecules cm^{-3} at Bresso. The OH-radical levels in relation to the NO_x concentrations at these two sites are within the range of results from measurements or estimates in other experiments [Daum *et al.*, 2000; Volz-Thomas and Kolahgar, 2000].

[43] Sensitivity analyses showed that HONO is a rather important parameter in our calculations. As described by Stutz *et al.* [2002], the HONO concentrations recorded at Bresso can be reasonably explained by steady state calculations and it is unlikely that HONO exceeds 5% of NO₂ concentration during daytime. At the Verzago site, measurements of HONO were performed with a denuder instrument. Since these measurements often exceeded 5% of the NO₂ concentration during daytime, we assume that this HONO measurement suffered from artifacts. We therefore calculated HONO concentrations according to Alicke *et al.* [2002] and used these values as inputs for the SSA.

[44] A comparison was made between SSA calculations which used observed NO and NO₂ as inputs with calculations that used only observed NO. Observed NO₂ is close to the calculated steady state value. The two types of calculations yield nearly identical predictions for other calculated quantities such as P(O₃). Furthermore, box model calculations were performed for testing our steady state assumption: Using measured concentrations as initial conditions for the box model, the NO to NO₂ ratio did not change significantly. We interpret it as meaning that the air at Verzago was close to being in steady state for radicals and NO₂.

[45] The comparison of measured and calculated peroxy radical concentrations (Figure 7) gives an ambiguous picture, mainly because the amount of data for comparisons is limited.



Figures 6. OH concentrations as calculated with SSA for Verzago and Bresso. (left) Average over 6 days (error bars are standard deviations). (right) OH concentrations in dependence of NO_x concentration (solid symbols denote noon values). See color version of this figure at back of this issue.

The only days where MCA data and complete input data sets for the SSA were available are 1, 5, and 8 June. On the morning of 5 June and on 8 June, calculated and observed peroxy radical concentrations are within the measurement and calculation errors. On 1 June, observed peroxy radicals are ~3–5 times of calculated values, a discrepancy that is much greater than expected based on a consideration of experimental and model errors. A maximum ozone production rate of 14 ppb h⁻¹ is predicted from equation (6) using calculated SSA values for peroxy radical concentration. An ozone production rate in excess of 50 ppb h⁻¹ is predicted from observed peroxy radical concentration. June 1 was a day with a relatively low O₃ concentration as compared with other IOP days, and on this basis the measured peroxy radical concentration appears to be too high. We suspect interferences in the peroxy radical measurement as suggested by *Stevens et al.* [1997], who applied comparable measurement and calculation methods and found similar discrepancies in environments with relatively high NO_x levels (NO > 100 ppt).

4.1.2. Sensitivity of O₃ Production to NO_x and VOC

[46] For all data sets we calculated the relative change of the ozone production rate due to a small change (5%) in the concentrations of NO_x and VOC (including CO, biogenics and CH₄). In Figure 8 these relative ozone production sensitivities (dlnP(O₃)/dln [NO_x] and dlnP(O₃)/dln[VOC]) are plotted against the parameter L_N/Q.

[47] The L_N/Q values calculated from observations (circles and squares) follow the theoretical pattern (lines) quite well, except at higher L_N/Q values, where the ‘observed’ relative sensitivity of VOC changes is somewhat lower than in theory. However, the transition between NO_x and VOC sensitive O₃ production occurs almost exactly at the theoretical L_N/Q value of 0.5. L_N/Q is therefore used in the following to distinguish between NO_x- and VOC sensitive ozone production. Calculated L_N/Q values for the sites of Bresso and Verzago reveal that ozone production at the urban site of Bresso is VOC sensitive, while Verzago exhibited both VOC and NO_x sensi-

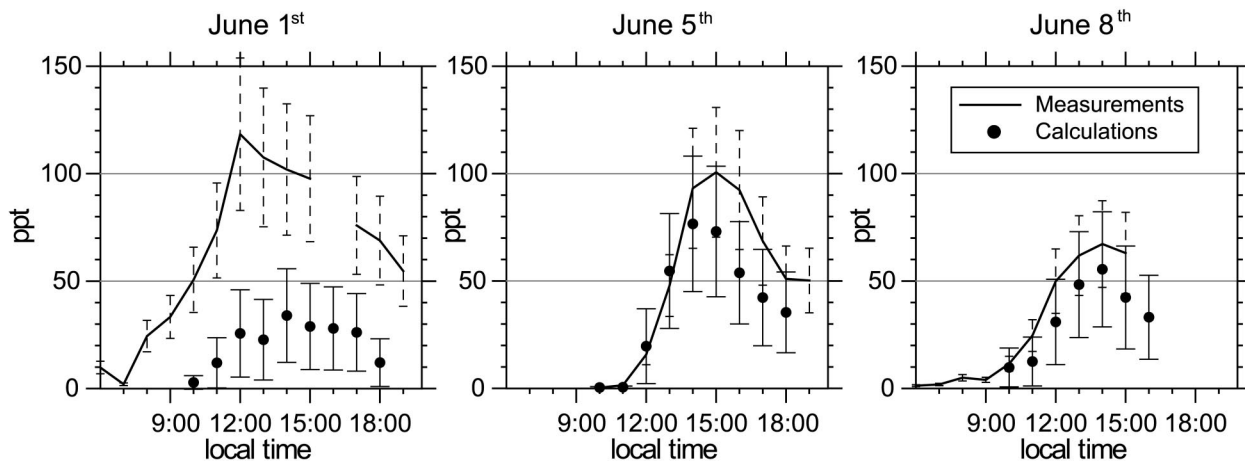


Figure 7. Comparison of peroxy radical measurements (lines) and calculations (symbols) at Verzago. Measurement uncertainties are 39%; error bars of the calculations were determined from errors of the concentrations used as input for the SSA by assuming standard error propagation.

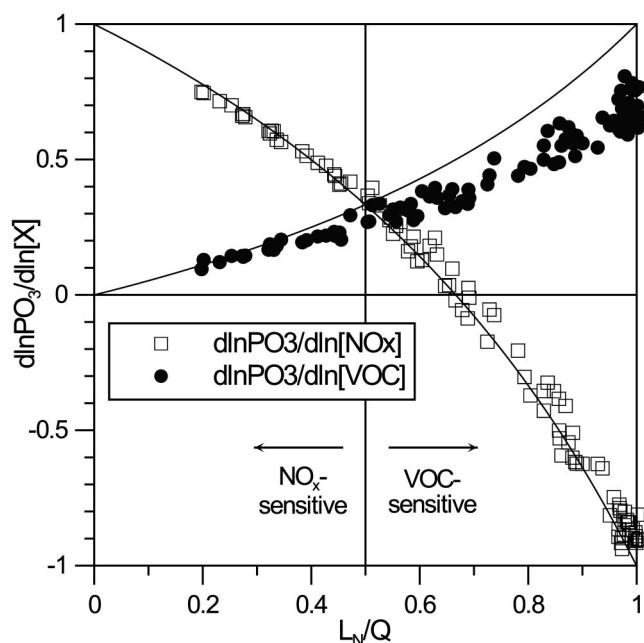


Figure 8. Relative sensitivities of local ozone production as determined from measurements between 1000 and 1800 at Bresso and Verzago.

tive conditions. The VOC sensitivity at Bresso is not surprising due to the various strong emission sources nearby. The situation in Verzago is more complex. Ozone production and its sensitivity is influenced by the diurnal variation of radiation, vertical mixing and horizontal transport processes. Figure 9 shows the ozone productions and their sensitivities at Verzago for 6 IOP days. In the morning, ozone production is generally VOC sensitive. Lower radiation results in a smaller radical production and the lower height of the boundary layer limits vertical mixing. Therefore there is a large amount of NO_x relative to radical production, most radicals will be removed by NO_x - radical reactions, and L_N/Q will be close to 1 and O₃ production will be VOC-sensitive.

[48] The days 12 and 13 May were similar, considering the solar radiation (sunny, no clouds), but the local ozone production at Verzago shows a rather distinctive behavior. At 1400 it was NO_x-sensitive on 12 May but VOC-sensitive on 13 May. The maximum O₃ production rate on 13 May occurred significantly later than the radiation maximum and was between 5 and 10 ppb higher than the day before. For most of the measured species at Verzago, a dramatic increase in concentration was observed between 1300 and 1400 local time, indicating the arrival of a heavily polluted air mass (Figure 3). Wind measurements by the wind profiler in Seregno reveal that the wind directions were directly from the South on 13 May, but more western on 12 May (Figure 2). It appears that a strong emission source south of Verzago (other than Milan) causes this difference between the situations on 12 and 13 May. A comparison of the quasi conservative tracers, CO and NO_y, registered during 13 May in Bresso, Seregno, and Verzago also points to a substantial emission source between Bresso and Verzago in addition to the strong emissions in the metropolitan area of Milan [cf. Martilli *et al.*, 2002]. Our local analysis reveals that this plume caused an additional ozone production of 5–10 ppb h⁻¹. Furthermore, the sensitivity of ozone production during this event was more VOC sensitive (higher L_N/Q) than at the

same time on other IOP days. In the absence of a pronounced plume, O₃ production at Verzago was NO_x-limited on cloudless days. Recall that the sum of VOC and the reaction rate of VOC + OH as used in our calculation represent lower limit estimates. An increase in VOC concentrations and reactivity would shift the results toward more NO_x sensitivity.

4.2. Lagrangian Model Runs

[49] In the previous section we presented an analysis of the instantaneous state of an air parcel. For the development of an O₃ control strategy, the sensitivity of O₃ concentration to an emissions change has to be considered. This quantity will depend on the history of the air mass. With the help of model calculations we will discuss how representative our surface based analysis can be and whether statements about the local ozone production rate can be linked to the regional question of the effects of emission controls.

[50] The Lagrangian model described in section 3 was used to simulate the concentrations observed at Verzago on 13 May. A comparison between model results and measurements at Verzago is shown in Figure 10. The model simulates reasonable O₃ concentrations and captures approximate levels of other photooxidants. However, a 1-D model cannot accurately simulate 3-D transport, and there are known deficiencies in model inputs. For example, the difference in CO is most likely a consequence of insufficient emissions in the inventory, as pointed out by Thielmann [2000]. On the other hand, SO₂ emissions seem to be much too high [Martilli *et al.*, 2002]. The model reproduces similar NO_x and VOC levels but fails to simulate the high concentrations observed in the early afternoon. These differences might be explained by the modest spatial resolution of emissions (9 × 9 km) used for these model calculations. However, there is also evidence from ground and airborne measurements that there are some hot spots in the emissions that are not sufficiently resolved in the inventory.

[51] HNO₃ concentrations are much higher in the model since it does not include aerosol formation. If the sum of HNO₃ and aerosol NO₃⁻ measurements (dashed line in Figure 10) are compared to modeled HNO₃ values, the agreement is reasonable.

[52] Isoprene measurements taken at the surface are known to be representative for only a very limited area [Staffelbach *et al.*, 1997a]. Because of its high reactivity toward OH, isoprene is quickly removed and concentrations are dominated by local emissions. Isoprene measurements taken on an aircraft 500 m above ground agree well with mean mixing layer concentrations in the model. It is therefore concluded that the isoprene emissions of the emission inventory are realistic. Since the modeled concentrations are higher than the surface measurements, it is likely that the measurement site exhibited lower isoprene emissions nearby than the average of the corresponding grid cell in the emission inventory. The evening peak of isoprene was a repeatedly observed phenomenon at the Verzago site. We rule out an anthropogenic origin, since there is no correlation between the concentrations of toluene and isoprene or benzene and isoprene during the evening hours (whereas there is a correlation between toluene and benzene). Elevated isoprene concentrations during the evening at surface sites have been observed at various locations [Stroud *et al.*, 2001; Starn *et al.*, 1998, and references therein]. We assume a similar explanation for the Verzago site: The development of a shallow nocturnal boundary layer in combination with a higher lifetime of isoprene due to reduced OH levels in the evening leads to elevated concentrations even

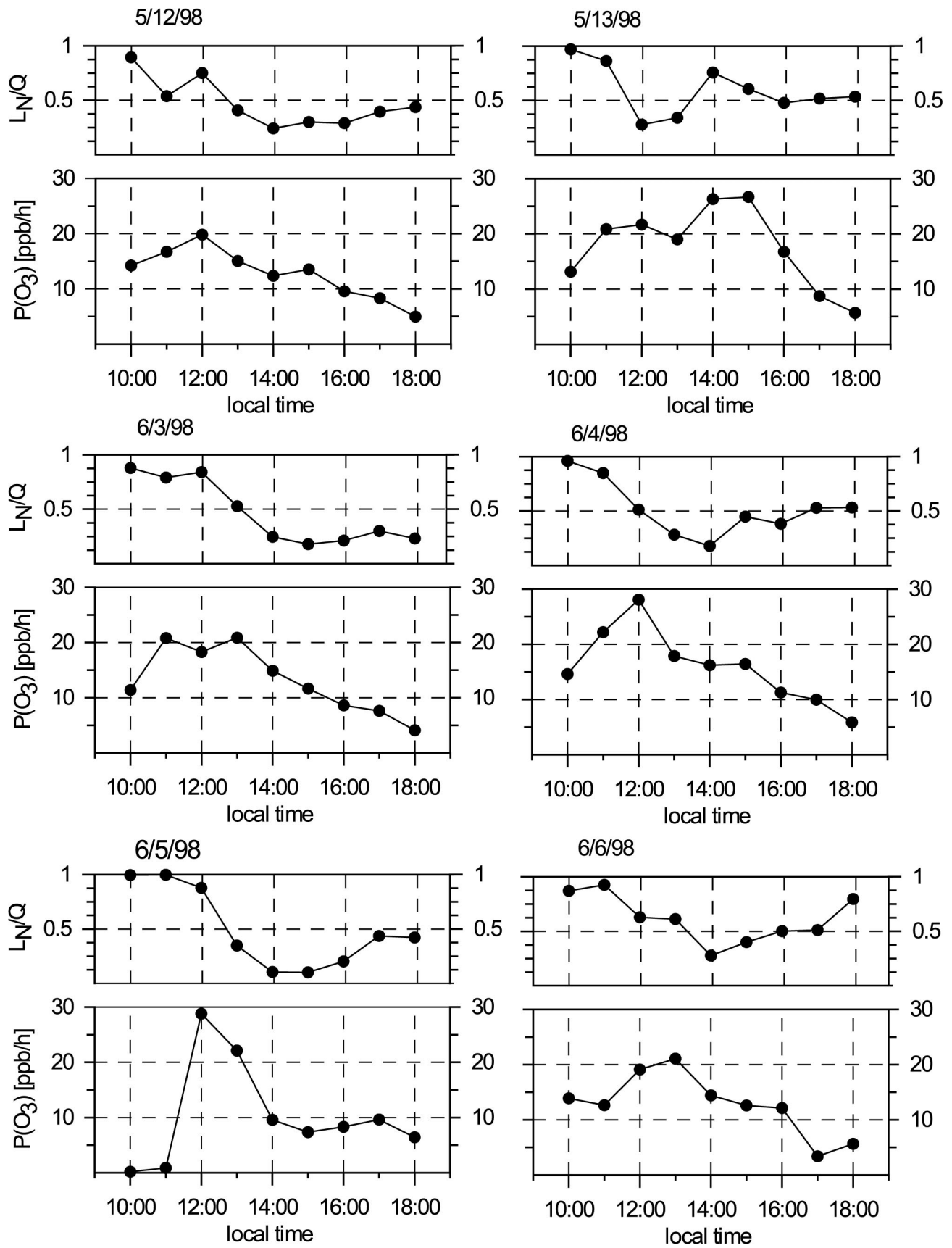


Figure 9. Instantaneous ozone productions and their sensitivities (expressed by L_N/Q) to NO_x and VOC concentrations. SSA results from measurements at Verzago.

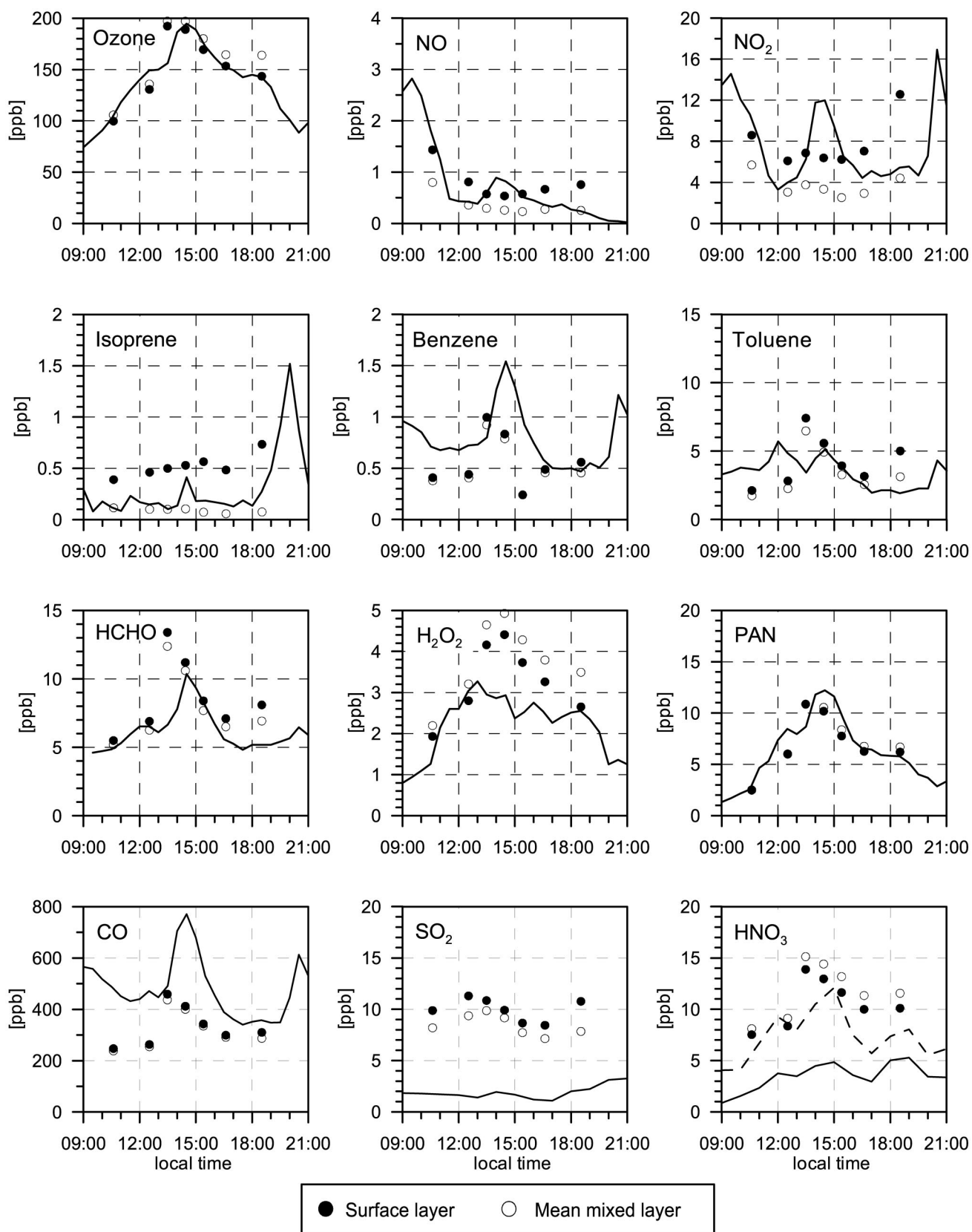


Figure 10. Simulation of the situation on May 13, 1998: Measurements (lines) at Verzago and concentrations predicted by the Lagrangian model (symbols) at the arrival of the seven trajectories at Verzago.

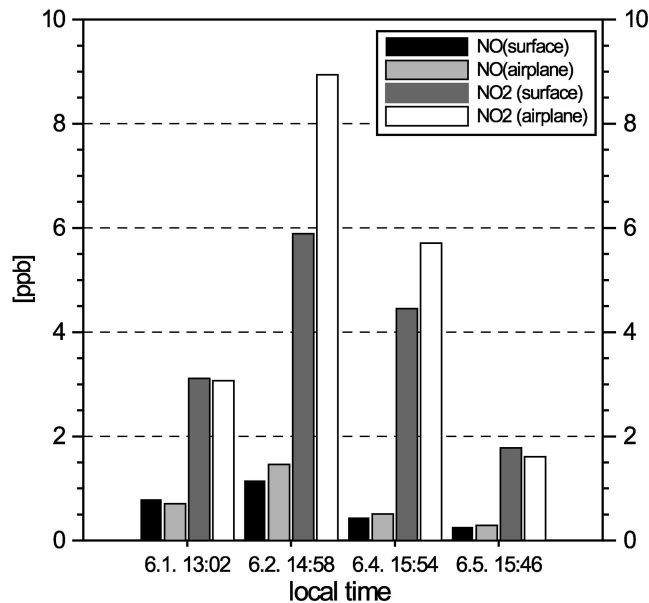


Figure 11. Comparison of surface and airplane NO_x measurements at Verzago.

though emissions are lower than in the middle of the day. Again, this phenomenon is beyond the resolution of our Lagrangian model and can therefore not be realistically represented in the simulation.

[53] Since the measured NO_x and VOC levels compare well to the afternoon concentrations modeled for the mean of the mixing layer, it is concluded that Verzago is a station representing well the conditions of the mixing layer. This is supported by NO_x measurements at 200–700 m above ground on the French ARAT aircraft. When flying directly above Verzago, the NO_x levels recorded on the aircraft are in the range of those registered at the surface (Figure 11).

[54] In order to examine the treatment of vertical mixing in

the model, radon was included as a modeled species and compared to measurements. For radon a decay constant of $2.1 \times 10^{-6} \text{ s}^{-1}$ (i.e., a half-life period of 3.82 days) and a constant emission rate of 72 Bq m^{-2} was used. Figure 12 shows modeled and measured radon values for 13 May and indicates that vertical mixing in the model was simulated reasonably well.

[55] The comparisons between model runs and measurements demonstrate that the model simulated a situation that is realistic for the Po valley. It is therefore a useful tool for considering the relations between local and integrated ozone production sensitivities.

5. O₃ and P(O₃) Along a Trajectory

[56] In this section the Lagrangian model is used to show how the sensitivity of O₃ concentration to an emissions reduction of NO_x or VOCs varies as a function of time and altitude as an air mass is advected along a trajectory. As a case study, we choose the trajectory simulating the air mass reaching Verzago at 1530 local time. The response of O₃ to an emissions change is determined by comparing a base case calculation with a calculation having either a 35% NO_x or VOC (including CO, CH₄, and biogenic VOC) reduction.

[57] A steady state analysis has also been done following the methods of section 3, but using Lagrangian model output in place of real observations. The SSA yields predictions of the sensitivity of P(O₃) to NO_x and VOCs. We compare the local sensitivity of P(O₃) to NO_x and VOC with the integrated sensitivity of O₃ concentration to NO_x and VOCs emissions. The purpose of this comparison is to determine the ability of the local analysis to predict the effects of an emissions change.

5.1. Response of O₃ to an Emissions Change

[58] Figure 13 shows the calculated near-surface O₃ concentration in an air parcel that is advected to the north from Milan to Verzago. In the morning the air parcel is over downtown Milan; it reaches Verzago at 1530 and at later times it is north of Verzago. The three lines in Figure 13 are for base case

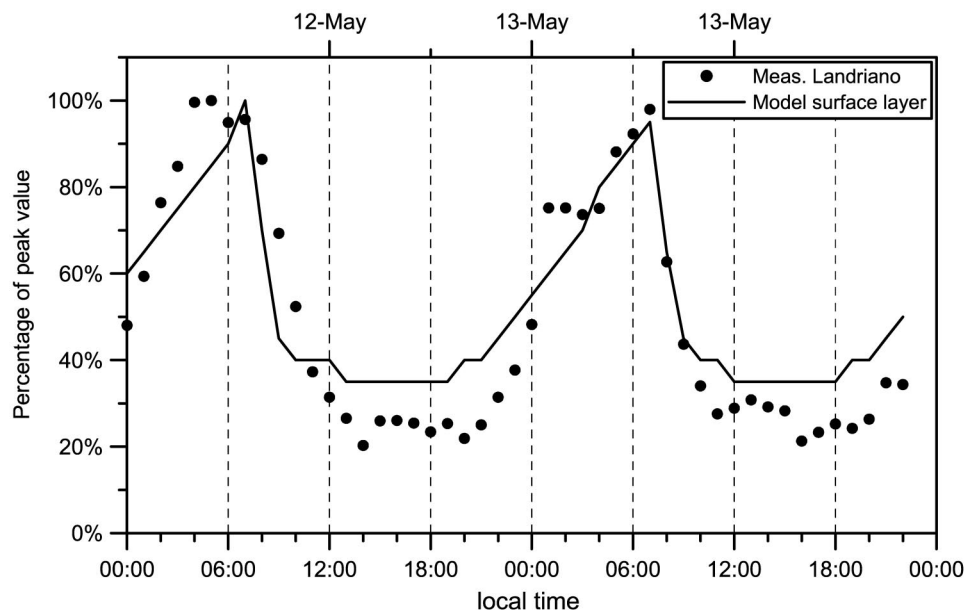


Figure 12. Radon concentrations measured at Landriano on May 13 and in surface layer of the 1-D model. Concentrations are scaled to daily peak values.

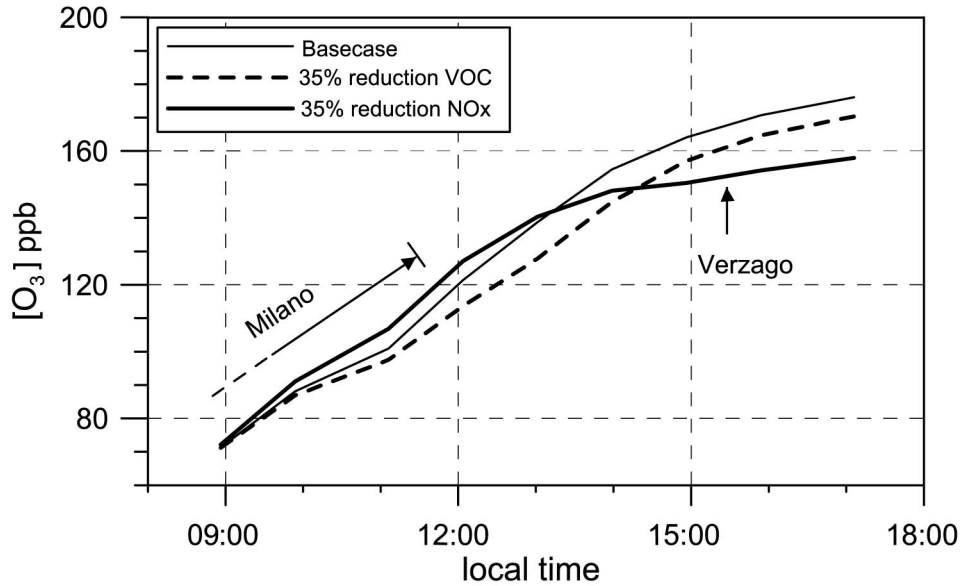


Figure 13. Ozone as predicted by the Lagrangian model: Surface concentrations of an air column advected northward from Milan toward Verzago. It moves over the urban area of Milan from 0800 to 1130 and then heads north with a speed of 8 to 10 km h⁻¹.

emissions and for NO_x and VOC emissions reduced by 35%. Before 1300 a NO_x reduction is seen to cause a higher near surface (model layer 1) O₃ concentration. At about 1430, when the air mass is 30 km north of downtown Milan, the NO_x and VOC reduction curves cross. Before this time, O₃ is VOC-sensitive, and after this time, it is NO_x-sensitive. Thus the air parcel displays the expected transition from VOC sensitive chemistry near a source region to NO_x sensitive chemistry downwind.

[59] The dependence of NO_x versus VOC sensitivity on altitude is illustrated in Figure 14. When $[O_3](NO_x \text{ reduc-})$

tion) – $[O_3](VOC \text{ reduction})$ is greater than zero, a VOC emissions reduction is more effective than a NO_x emissions reduction in reducing O₃. By definition, O₃ is then VOC-sensitive. At all times, NO_x sensitivity increases with altitude. In the uppermost layer the ozone concentration remains NO_x sensitive throughout the whole trajectory. The switch from VOC to NO_x sensitivity occurs ~30 min later at the surface than in the middle of the mixed layer. Later in the day, the sensitivity in all six model layers converge. Convective mixing aided by the absence of a strong surface emission source leads to a well mixed atmosphere.

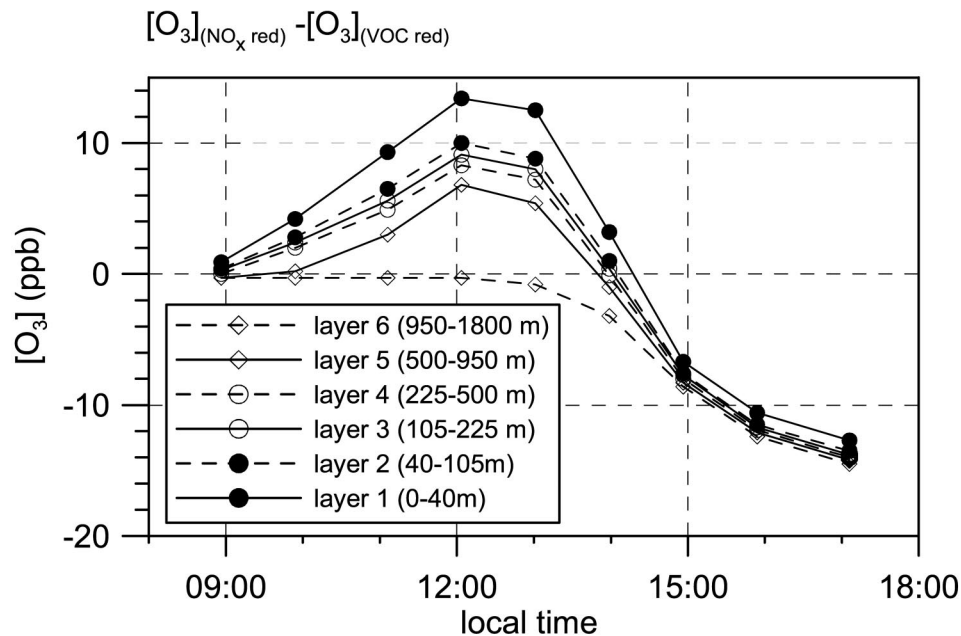


Figure 14. Modeled ozone concentrations at different altitudes: Difference between scenarios with 35% reduced NO_x and VOC emissions.

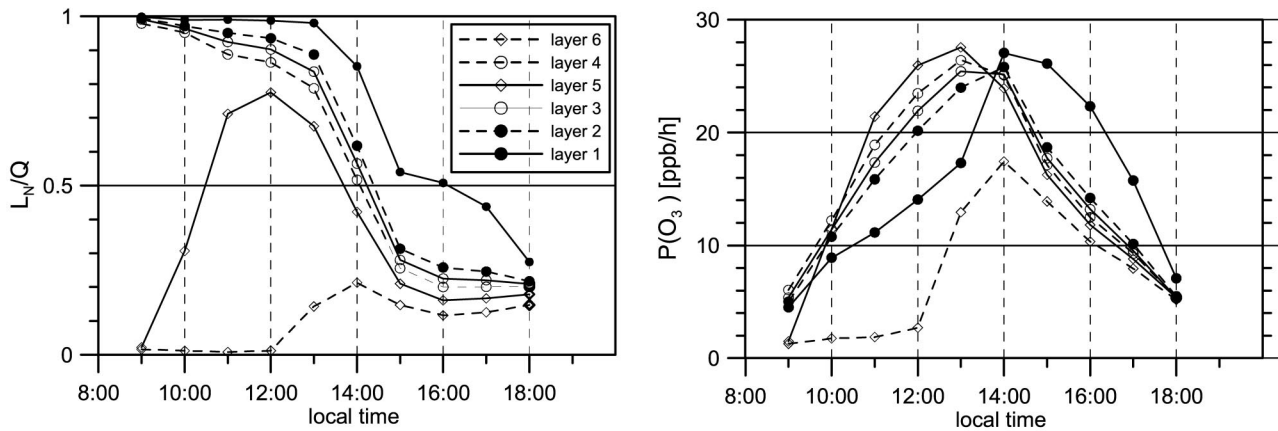


Figure 15. Characterization of instantaneous ozone productions along the model trajectory. Results of the SSA using concentrations of the 1-D model as inputs. (a) O₃ production and (b) sensitivity of O₃ production expressed by L_N/Q .

5.2. Base Case Ozone Production Rate

[60] Output from the Lagrangian model was used to calculate $P(O_3)$. Two ways of doing this were explored. In one method, Lagrangian model results (for nonradical species) were used as input to an SSA calculation identical to that described in section 3.1. The SSA calculation then yields predicted values for radical concentrations. In the other approach, radical concentrations are obtained directly from the Lagrangian calculation. In both cases, $P(O_3)$ is calculated from $[NO]$, $[HO_2]$, and $[RO_2]$ using equation (6). A comparison between these two methods is discussed at the end of this section.

[61] $P(O_3)$ calculated from Lagrangian model output using the SSA method is shown in Figure 15. The SSA calculations also yield values for L_N/Q , which according to (7–8) and Figure 8, are directly related to $P(O_3)$ sensitivities. Figure 15 illustrates how the instantaneous ozone production rates depend on altitude and how they evolve as the air mass is advected from a source region to a cleaner downwind region.

[62] In model layers 1–4, $P(O_3)$ starts the day VOC-sensitive ($L_N/Q > 0.5$) and becomes NO_x-sensitive ($L_N/Q < 0.5$) later in the day. Model layers 5 and 6 (500–1800 m above ground level) represent the residual layer early in the day. Because of low pollutant concentrations (in particular low NO_x concentrations), ozone production in layers 5 and 6 is very NO_x sensitive at the start of the day. When the boundary layer reaches heights within these model layers (see Figure 4), ozone production increases and gets more sensitive to the VOC concentration (i.e., L_N/Q increases). Later in the day when vertical mixing is well established, layers 2–6 exhibit rather similar conditions of ozone production, while the surface layer still exhibits a more VOC sensitive O₃ production. Part of the more VOC sensitive ozone production in the lowest layer is a consequence of the fact that the model receives its emission inputs continuously into that layer. NO_x levels in the surface layer are thus consistently higher than the average in the mixed layer. Test runs with anthropogenic emissions interrupted for 30 min show only a negligible difference between surface layer and the other layers within the mixing layer.

[63] The SSA calculation predicts that $P(O_3)$ is always NO_x-limited in layer 6 and that the transition between VOC and NO_x sensitivity occurs at about 1400 for model layers 2–5

and at 1600 for the surface layer. In the presence of surface emission sources, a prediction of $P(O_3)$ sensitivity based on surface data is thus different than a prediction based on the bulk of the boundary layer. Note also the height of each of the model layers increases with altitude so that the amount of ozone produced in the upper layers is greater than that produced in the lower layers even if the effective production rate (ppb/h) is lower.

[64] The analysis of $P(O_3)$ in different layers also allows us to demonstrate that the vertical model resolution can play a major role in the sensitivity of ozone production. Recall that turbulent mixing is parameterized by means of eddy coefficients between the model layers. Within the layers, complete and instantaneous mixing is assumed. When the boundary layer rises above the altitude of a model layer, mixing from underneath into the upper model layer will occur and any pollutants lifted up are distributed homogeneously within this layer. As a consequence, vertical mixing at certain altitudes will be faster in the model than in reality. This difference rises with increasing layer dimensions of the model. In our case, this effect becomes particularly pronounced when the boundary layer grows through the uppermost layer (which has a vertical dimension of 850 m). This occurs between 1100 and 1400. NO_x and VOC transported into this layer with its strongly NO_x sensitive ozone production leads to a significant increase in the ozone production. Considering the total ozone production in the column, the poor vertical resolution of the model thus has the effect, that more ozone is produced under NO_x-sensitive conditions. Even though the modest vertical resolution of our model unrealistically exaggerates this effect, it demonstrates that entrainment is an important factor in the study of ozone production sensitivities. That a model is successful in reproducing the conditions for O₃ production at the surface, does not necessarily imply that it is equally skilled at simulating conditions in the upper part of the mixed layer. Model studies about the limitation of ozone production therefore should be carefully tested not only against surface measurements, but also against observations throughout the boundary and the residual layer. Measurements of entrainment fluxes would be very helpful in future field studies addressing the limitation of ozone production.

5.3. Comparisons Between P(O₃) and O₃

[65] Calculations presented in the last two subsections yield predictions for (1) O₃ concentration and production rate P(O₃), (2) the sensitivity of P(O₃) to changes in the concentration of NO_x and VOCs, and (3) the change in O₃ concentration due to a change in emissions. We are now in a position to offer some qualitative observations about how these quantities are related.

[66] In the Lagrangian calculation, O₃ concentration is affected by chemical production and loss, mixing between model layers, and surface deposition. Leaving aside mixing as not affecting the total amount of O₃ and noting that chemical loss and surface loss are relatively small, the amount of O₃ formed over the calculation (between initial time t₀ and ending time t) should be approximately equal to the amount of O₃ chemically produced, or

$$[O_3(t)] - [O_3(t_0)] = \int P(O_3) dt. \quad (9)$$

Equation (9) can be differentiated with respect to the NO_x or VOC emission rate, E_{NO_x} or E_{VOC}, yielding

$$\frac{d[O_3]}{dE} = \int \frac{dP(O_3)}{dE} dt, \quad (10)$$

where E is either E_{NO_x} or E_{VOC}. Although P(O₃) can be calculated from local observations, dP(O₃)/dE cannot. This derivative represents the response of the instantaneous state of the atmosphere to an emissions change which took place at a different location and at an earlier time. We can attempt to simplify equation (10) by expanding the derivatives using the chain rule.

$$\begin{aligned} \frac{d[O_3]}{dE} = & \int \left(\frac{\partial P(O_3)}{\partial [NO_x]} \frac{\partial [NO_x]}{\partial E} + \frac{\partial P(O_3)}{\partial [VOC]} \frac{\partial [VOC]}{\partial E} \right. \\ & \left. + \frac{\partial P(O_3)}{\partial Q} \frac{\partial Q}{\partial E} \right) dt. \end{aligned} \quad (11)$$

[67] The chain rule expansion is done assuming that there are three independent variables, NO_x, VOCs, and Q (odd-H production) that provide a complete description of local photochemistry. An actual evaluation of the integrand in equation (11) would be problematic as, for example, HCHO is both a radical source and a VOC. Rather than deal with the exact form of equation (11) we consider some general features. Equation (11) contains terms like $\partial[NO_x]/\partial E_{NO_x}$ and $\partial[VOC]/\partial E_{NO_x}$ which express how an emission change affects [NO_x] and [VOC] downwind. In the simplest case an emission change of (for example) NO_x would cause a proportionate change in NO_x downwind and no change in [VOC] or Q. Then,

$$\frac{d[O_3]}{dE_{NO_x}} = \int \frac{\partial P(O_3)}{\partial [NO_x]} dt \quad (12a)$$

$$\frac{d[O_3]}{dE_{VOC}} = \int \frac{\partial P(O_3)}{\partial [VOC]} dt. \quad (12b)$$

[68] Equation (12) suggests that, to a first approximation, O₃ concentration sensitivity depends on the time integral of local ozone production sensitivity. If equations (12a) and (12b) are correct, then the transition of [O₃] from being VOC-sensitive to NO_x-sensitive should occur at a time when, roughly speaking, the VOC-sensitive contribution of P(O₃) balances the NO_x-sensitive contribution. Since P(O₃) is VOC-sensitive

at the beginning of the trajectory and switches to NO_x-sensitive at about 1400 (see Figure 15 for layers 2–5, where most of the O₃ is produced), we would anticipate that the change from VOC to NO_x sensitivity for ozone concentration would occur several hours later, at a time when enough O₃ is formed under NO_x-sensitive conditions at the end of the trajectory to balance the O₃ formed under VOC-sensitive conditions at the start of the trajectory. However, in this case the shift of the ozone concentration sensitivity occurs about at the same time (1400), as can be seen from Figure 13. Adding in the effects of level 6, which remains NO_x-sensitive throughout the day, gives us a somewhat earlier layer-average transition time for P(O₃) to become NO_x sensitive. Even still, it is clear that at 1400 (when O₃ makes the transition) less than half of the O₃ has been formed under NO_x-sensitive condition according to the base case calculation. Therefore P(O₃) from the base case calculation yields a prediction the [O₃] is more VOC-sensitive than it actually is.

[69] P(O₃) along a trajectory does not give us a quantitative prediction of the VOC to NO_x sensitive transition of [O₃] because equation (12) is only an approximation. NO_x and VOC concentration depend in a nonlinear way on their emissions. A certain reduction of NO_x emissions will not only result in a different decrease in its concentration, but it will also influence the VOC concentration (and vice versa). Because of the complicated and nonlinear dependence of [NO_x] and [VOC] on emissions, d[O₃]/dE_{NO_x} and d[O₃]/dE_{VOC} cannot be described as simple functions of P(O₃) as written in equation (12).

[70] We can explicitly demonstrate the effects of the nonlinear relation between [NO_x] and [VOC] and their emissions by examining P(O₃) for the calculations in which emission rates of NO_x and VOCs were reduced by 35%. Figure 16a shows the difference in O₃ production rate (calculated with the SSA method) for the two emission reduction scenarios,

$$\Delta P(O_3) = P(O_3)_{NO_x \text{ reduction}} - P(O_3)_{VOC \text{ reduction}}. \quad (13)$$

A comparison of the zero-crossing in Figure 16a with the L_N/Q = 0.5 line in Figure 15, shows that the P(O₃) transition from VOC to NO_x sensitivity occurs almost an hour earlier in the day when the effect of emissions reduction on [NO_x] and [VOC] is taken into account.

[71] In Figure 16b, ΔP(O₃) is calculated directly from the Lagrangian model using predicted values for [NO], [HO₂], and [RO₂]. Ideally, this method would yield the same results as the SSA method but there are differences because of approximations made in the SSA method. The most serious of these approximations is the assumption that PAN is in steady state. Figure 10 shows that PAN concentrations are high and therefore its formation and eventual dissociation, both of which are not part of a steady state calculation, can have a significant influence on local photochemistry. Figure 16b indicates that an earlier transition time is obtained when P(O₃) is calculated directly from the Lagrangian model. Near the transition time, the Lagrangian calculation predicts that the atmosphere is more NO_x sensitive than does the SSA calculation. We have traced this effect to the importance of PAN chemistry: At the time that model levels 2–4 make a transition from VOC to NO_x sensitive behavior, the production rate of PAN is positive, which implies that fewer radicals are available for forming HNO₃. As Sillman [1995] has noted, the transition point from VOC to NO_x sensitivity depends on P(HNO₃) and not on P(PAN). This result is also implicit in the derivation given by Kleinman *et al.* [1997] in which analytic equations for NO_x and

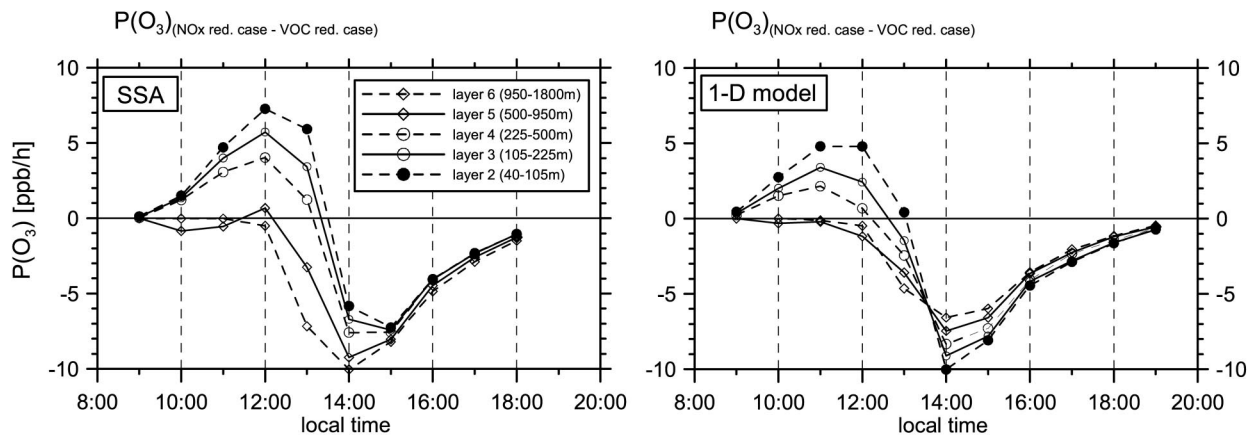


Figure 16. Differences in ozone production between runs with 35% reduction of NO_x and VOC emissions. (a) Steady state calculations with 1-D model concentrations as inputs; (b) 1-D model results.

VOC sensitivity (equations (7) and (8) of this paper) follow from an argument in which L_N is approximated as $P(\text{HNO}_3)$. The SSA calculation by neglecting the PAN formation pathway for removing radicals, overestimates $P(\text{HNO}_3)$ and $P(\text{HNO}_3)/Q$ in regions where PAN is being formed. It therefore overpredicts VOC sensitivity. In regions where PAN is dissociating, the SSA calculation overpredicts NO_x sensitivity.

6. Conclusions

[72] As part of the 1998 PIPAPO field campaign to study the Milan urban plume, comprehensive sets of trace gas measurement were made downwind at Bresso and Verzago. These observations were used as input to a steady state calculation for the purpose of determining the concentration of free radicals, the production rate of O₃, $P(\text{O}_3)$, and the sensitivity of $P(\text{O}_3)$ to NO_x and VOCs.

[73] The SSA calculations show that $P(\text{O}_3)$ at Bresso was VOC-sensitive. In contrast, $P(\text{O}_3)$ at Verzago exhibited both VOC and NO_x sensitive behavior, usually starting out in the morning as VOC sensitive and becoming NO_x sensitive in the early afternoon. Maximum rates for O₃ production were about 30 ppb h⁻¹ at Verzago.

[74] This observation based analysis allows us to determine how $P(\text{O}_3)$ is affected by changes in NO_x and VOCs, but it does not give us an answer to the question of how O₃ concentration depends on emissions. A study with a Lagrangian model was performed to address the later problem. By looking at the instantaneous ozone productions along this model case, we could illustrate how local ozone production sensitivities relate to ozone concentration sensitivities.

[75] We found a vertical gradient in $P(\text{O}_3)$ sensitivity with model layers near the ground being more VOC sensitive than layers in the midboundary layer. Since ozone production at the surface accounts only for a fraction of the ozone concentration, local analyses based on surface observations need careful interpretation. Conditions at a surface site will only be representative for a large part of the ozone production if the site is not affected by local emissions and at times when strong vertical mixing is established.

[76] The nonlinear relationships between emissions and concentrations prevent a direct derivation of ozone concentration sensitivity from local sensitivities of ozone production. Calculations with chemical transport models are necessary for

predictions about the sensitivity of ozone concentrations. In our simulation of the situation on 13 May, $P(\text{O}_3)$ in mid of the mixed layer makes a transition from VOC sensitive behavior to NO_x sensitive behavior at about the same time as O₃ concentration changes from being VOC sensitive to NO_x sensitive. Recalling the results of the local analyses at the Verzago site on this day, it is plausible that ozone concentration during the plume arrival was VOC sensitive, but NO_x sensitive later in the afternoon.

[77] This finding fits with other analyses during the PIPAPO campaign [Martilli et al., 2002; Thielmann et al. 2002]. The Milan area exhibits only a limited area of VOC sensitive ozone concentration during summer smog episodes; the transition from VOC to NO_x-sensitive regime downwind of Milan occurs within 4–5 hours.

[78] **Acknowledgments.** We thank all participants who contributed their data to build the PIPAPO database. The help of various institutions of the Lombardy region for the organization of the campaign is highly appreciated. We thank Thomas Staffelbach for his commitment during the field experiment and his valuable inputs to our analyses. Financial support through the Swiss Agency for the Environment, Forests and Landscape (SAEFL) (Project “Biogene Aerosole”), and through the commission for technology and industry (KTI) (Eurotrac-2 project LOOP) is greatly acknowledged. The National Center for Atmospheric Research is sponsored by the National Science Foundation.

References

Alicke, B., U. Platt, and J. Stutz, Impact of nitrous acid photolysis on the total hydroxyl radical budget during the LOOP/PIPAPO study in Milan, *J. Geophys. Res.* 107, doi:10.1029/2000JD000075, in press, 2002.

Ashbourn, S. F. M., M. E. Jenkin, and K. C. Clemishaw, Laboratory studies of the response of a peroxy radical amplifier to HO₂ and a series of organic peroxy radicals, *J. Atmos. Chem.*, 29, 233–266, 1998.

Atkinson, R., D. L. Baulch, R. A. Cox, R. F. Hampson Jr., J. A. Kerr, and J. Troe, Evaluated kinetic and photochemical data for atmospheric chemistry, *J. Phys. Chem. Ref. Data*, 21, 1125–1600, 1992.

Cantrell, C. A., D. H. Stedman, and G. J. Wendel, Measurements of atmospheric peroxy radicals by chemical amplification. *Anal. Chem.*, 56, 1496–1502, 1984.

Daum, P. H., L. Kleinman, D. G. Imre, L. J. Nunnermacker, Y.-N. Lee, S. R. Springston, and L. Newman, Analysis of the processing of Nashville urban emissions on July 3 and July 18, 1995, *J. Geophys. Res.* 105, 9155–9164, 2000.

Fan, S. M., D. J. Jacob, D. L. Mauzerall, J. D. Bradshaw, S. T. Sand-

- holm, R. D. Blake, H. B. Sing, R. W. Talbot, G. L. Gregory, and G. W. Sachse, Origin of tropospheric NO_x over subarctic eastern Canada in summer, *J. Geophys. Res.*, *99*, 16,867–16,878, 1994.
- Grüebler, F. C., Reactive hydrocarbons in the Milan area: Results from the PIPAPO campaign, Ph.D. thesis, Swiss Fed. Inst. of Technol. (ETH), Zürich, 1999.
- Hastie, D. R., M. Weissenmayer, J. P. Burrows, and G. W. Harris, A calibrated chemical amplifier for atmospheric RO_x measurements, *Anal. Chem.*, *63*, 2048–2057, 1991.
- Heymann, M., Y. Kasas, and R. Friedrich, European emission data with high temporal and spatial resolution, in *Proceedings of EURO-TRAC Symposium 1994*, pp. 437–443, SPB Acad., Den Haag, Netherlands, 1994.
- Jacob, D. J., L. W. Horowitz, W. Munger, B. G. Heikes, R. R. Dickerson, R. S. Artz, and W. C. Keene, Seasonal transition from NO_x-to hydrocarbon-limited conditions for ozone production over the eastern United States in September, *J. Geophys. Res.*, *100*, 9315–9324, 1995.
- Kleinman, L. I., Ozone process insights from field experiments, part II, Observation based analysis for ozone production, *Atmos. Environ.*, *34*, 2023–2033, 2000.
- Kleinman, L. I., P. H. Daum, J. H. Lee, Y. Lee, L. J. Nunnermacker, S. R. Springston, and L. Newman, Dependence of ozone production on NO and hydrocarbons in the troposphere, *Geophys. Res. Lett.*, *24*, 2299–2302, 1997.
- Klimont, Z., M. Amann, J. Cofala, F. Gyarfas, G. Klaassen, and W. Schöpp, An emission inventory of the central European initiative 1988, *Atmos. Environ.*, *28*, 235–246, 1993.
- Lehning, M., H. Richner, and G. L. Kok, Pollutant transport over complex terrain: Flux and budget calculations for the POLLUMET field campaign, *Atmos. Environ., Part A*, *30*, 3027–3044, 1996.
- Madronich, S., and S. Flocke, The role of solar radiation in atmospheric chemistry, in *The Handbook of Environmental Chemistry*, edited by P. Boule, pp. 1–26, Springer-Verlag, New York, 1999.
- Martilli, A., A. Neftel, G. Favaro, F. Kirchner, S. Sillman, and A. Clappier, Simulation of the ozone formation in the northern part of the Po Basin, *J. Geophys. Res.*, *107*, doi:10.1029/2001JD000534, in press, 2002.
- Mihele, C. M., and D. R. Hastie, The sensitivity of the radical amplifier to ambient water vapour, *Geophys. Res. Lett.*, *25*, 1911–1913, 1998.
- Moore, W. B. D., S. P. Sander, D. M. Golden, R. F. Hampson, M. J. Kurylo, C. J. Howard, A. R. Ravishankara, C. E. Kolb, and M. J. Molina, Chemical kinetics and photochemical data for use in stratospheric modeling: Evaluation 10, *JPL Publ.*, *92–20*, 1992.
- Neftel, A., A. Blatter, R. Hesterberg, and T. Staffelbach, Measurements of concentration gradients of HNO₂ and HNO₃ over a semi-natural ecosystem, *Atmos. Environ.*, *30*, 3017–3025, 1996.
- Neftel, A., A. S. H. Prévôt, M. Furger, and B. Vogel, Overview paper PIPAPO special section, *J. Geophys. Res.*, *107*, doi:10.1029/2001JD001263, in press, 2002.
- Prévôt, A. S. H., J. Staehelin, G. L. Kok, R. D. Schillawski, B. Neininger, T. Staffelbach, A. Neftel, H. Wernli, and J. Dommen, The Milan photooxidant plume, *J. Geophys. Res.*, *102*, 22,375–23,388, 1997.
- Schultz, M., M. Heitlinger, D. Mihelcic, and A. Volz-Thomas, A calibration source for peroxy radicals with built-in actinometry using H₂O and O₂ photolysis at 185 nm, *J. Geophys. Res.*, *100*, 18,811–18,816, 1995.
- Sigg, A., A. Neftel, and P.K. Dasgupta, A miniaturized battery powered H₂O₂ monitor for airborne measurements in a motor glider, *Air Pollut. Res. Rep.*, *41*, 111–117, 1992.
- Sillman S., The use of NO_y, H₂O₂, and HNO₃ as indicators for ozone-NO_x-hydrocarbon sensitivity in urban locations, *J. Geophys. Res.*, *100*, 14,175–14,188, 1995.
- Staffelbach, T., and A. Neftel, Relevance of biogenically emitted trace gases for the ozone production in the planetary boundary layer in Central Europe, Swiss Fed. Res. Stn. for Agroecol. and Agric. (FAL), Zuerich-Reckenholz, Switzerland, 1997.
- Staffelbach, T., et al., Photochemical oxidant formation over southern Switzerland, 1, Results from summer 1994, *J. Geophys. Res.*, *102*, 23,345–23,363, 1997a.
- Staffelbach, T., A. Neftel, and L. W. Horowitz, Photochemical oxidant formation over southern Switzerland, 2, Model results, *J. Geophys. Res.*, *102*, 23,363–23,373, 1997b.
- Starn, T. K., P. B. Shepson, S. B. Bertman, D. D. Riemer, R. G. Zika, and K. Olszyna, Nighttime isoprene chemistry at an urban-impacted forest site, *J. Geophys. Res.*, *103*, 22,437–22,447, 1998.
- Stevens, P. S., et al., HO₂/OH and RO₂/HO₂ ratios during the Tropospheric OH Photochemistry Experiment: Measurement and theory, *J. Geophys. Res.*, *102*, 6379–6391, 1997.
- Stroud, C. A., et al., Isoprene and its oxidation products, methacrolein and methylvinyl ketone, at an urban forested site during the 1999 Southern Oxidants Study, *J. Geophys. Res.*, *106*, 8035–8046, 2001.
- Stutz, J., B. Alicke, and A. Neftel, Gradient measurements of NO₂ and HONO over grass in the urban atmosphere, *J. Geophys. Res.*, *107*, doi:10.1029/2001JD000390, in press, 2002.
- Thielmann, A., Sensitivity of ozone production derived from field measurements in the Po basin, Ph.D. thesis, Swiss Fed. Inst. of Technol. (ETH), Zürich, 2000.
- Thielmann, A., A. S. H. Prévôt, A. Neftel, and J. Staehelin, Sensitivity of ozone production derived from field measurements in the Italian Po basin, *J. Geophys. Res.*, *107*, doi:10.1029/2000JD000119, in press, 2002.
- Volz-Thomas, A., and B. Kolahgar, On the budget of hydroxyl radicals at Schauinsland during the Schauinsland Ozone Precursor Experiment (SLOPE), *J. Geophys. Res.*, *105*, 1611–1622, 2000.

J. Hjorth, Institute for Environment and Sustainability, Joint Research Center of the European Commission, I-21020 Ispra, Italy. (jens.hjorth@jrc.it)

L. I. Kleinman, Atmospheric Sciences Division, Department of Environmental Science, Brookhaven National Laboratory, Upton, NY 11973, USA. (kleinman@bnl.gov)

A. Neftel and C. Spirig (corresponding author), Swiss Federal Research Station for Agroecology and Agriculture, P.O. Box CH-8046, Zürich-Reckenholz, Switzerland. (albrecht.neftel@fal.admin.ch; chspirig@ucar.edu)

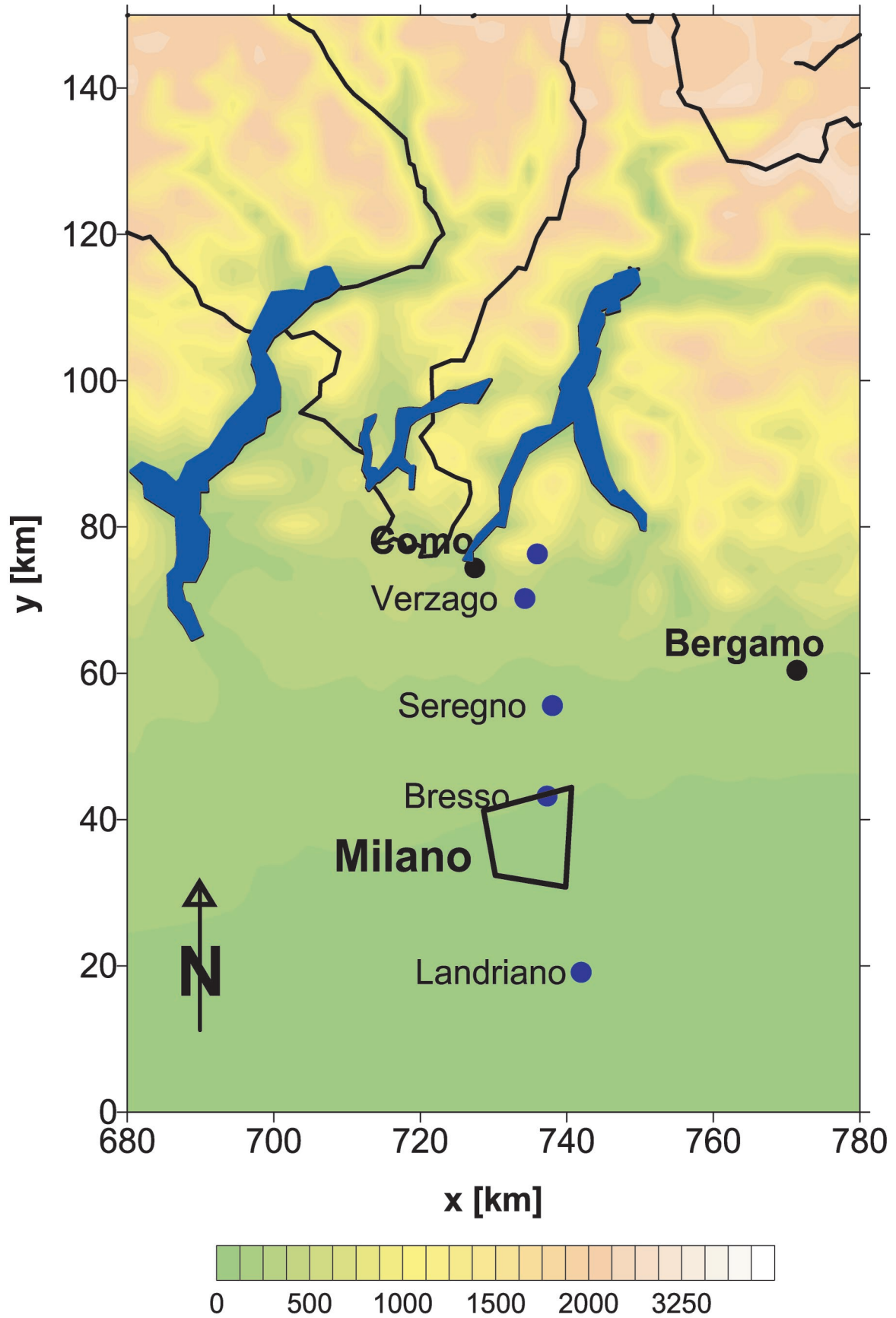
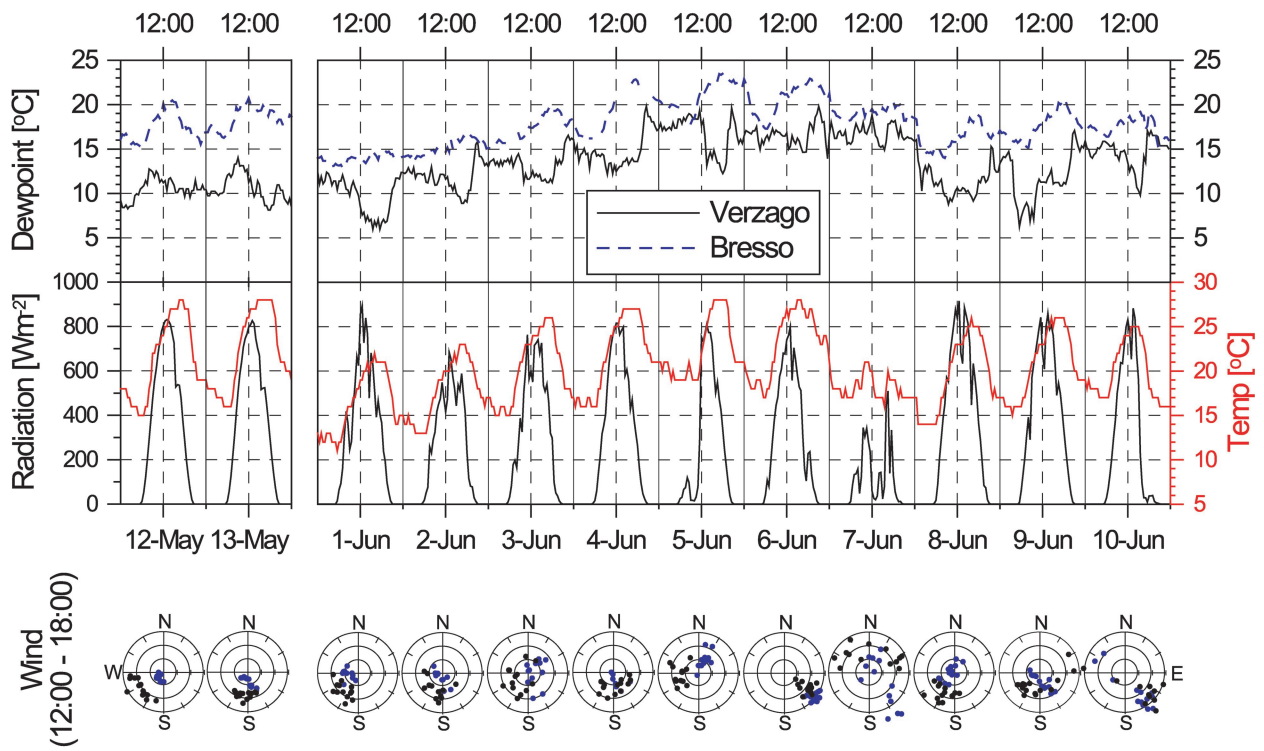


Figure 1. PIPAPO ground stations. Color scale indicates altitude above sea level (m).



Outer radius of polar plots corresponds to a wind speed of 3 ms⁻¹
Figure 2. Humidity, temperature (red), incoming radiation, and afternoon winds during the IOPs. Temperature and radiation are shown for Verzago only.

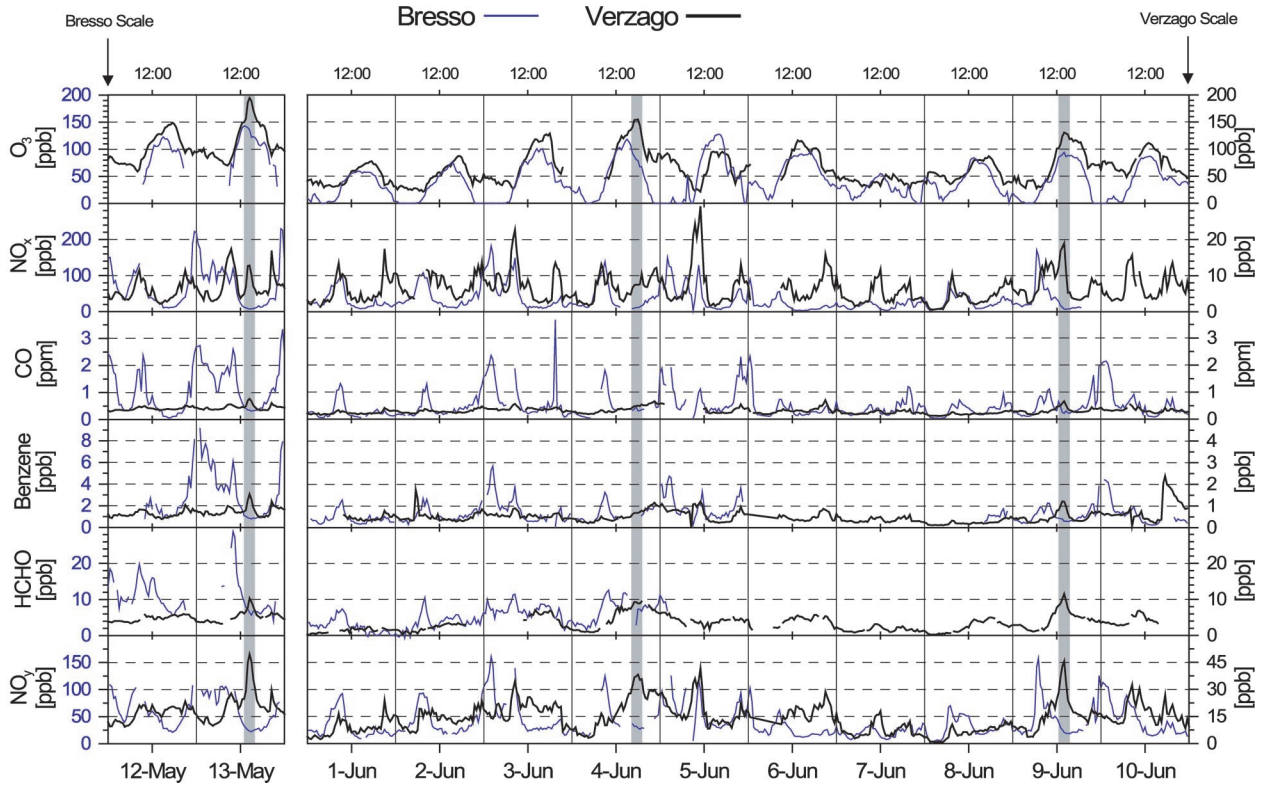
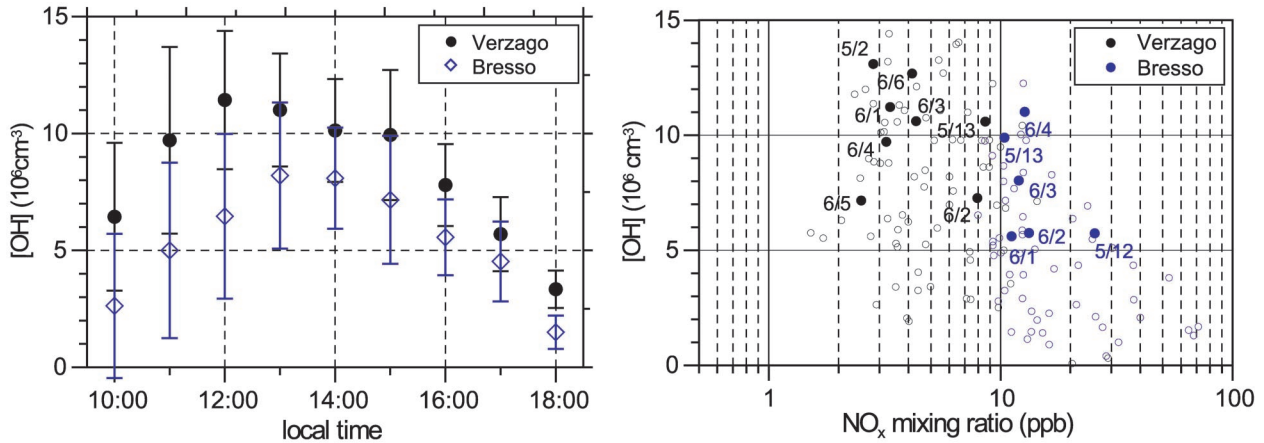


Figure 3. Selected measurements at Bresso and Verzago during both IOPs. Note the different scales at the two sites for NO_x, NO_y, and benzene. NO_x concentrations at Bresso during the afternoons of May 13, June 4, and June 9 are 35 to 40% of NO_y, whereas at Verzago the NO_x to NO_y ratio is 20 to 25%.



Figures 6. OH concentrations as calculated with SSA for Verzago and Bresso. (left) Average over 6 days (error bars are standard deviations). (right) OH concentrations in dependence of NO_x concentration (solid symbols denote noon values).